NATIONAL ADVISORY COMMITTEE FOR AERONAUTICS

TECHNICAL NOTE 2952

IMPINGEMENT OF WATER DROPLETS ON NACA 65_1-208 AND 65_1-212 AIRFOILS AT 4° ANGLE OF ATTACK

By Rinaldo J. Brun, Helen M. Gallagher, and Dorothea E. Vogt

Lewis Flight Propulsion Laboratory
Cleveland, Ohio

Washington
May 1953

NATIONAL ADVISORY COMMITTEE FOR AERONAUTICS

TECHNICAL NOTE 2952

IMPINGEMENT OF WATER DROPLETS ON NACA 65_1-208 AND 65_1-212 AIRFOILS AT 4° ANGLE OF ATTACK

By Rinaldo J. Brun, Helen M. Gallagher, and Dorothea E. Vogt

SUMMARY

The trajectories of droplets in the air flowing past an NACA 65_1-208 airfoil and an NACA 65_1-212 airfoil, both at an angle of attack of 4°, were determined. The amount of water in droplet form impinging on the airfoils, the area of droplet impingement, and the rate of droplet impingement per unit area on the airfoil surface affected were calculated from the trajectories and are presented herein to cover the following range of conditions:

Variable	Minimum value	Maximum value
Droplet diameter, microns	5	100
Airplane speed, mph	150	Critical flight speed
Altitude, ft	1000	35,000
Chord length, ft	2	20

The amount, extent, and rate of impingement of the NACA 65_1-208 airfoil are compared with the results for the NACA 65_1-212 airfoil. Under similar conditions of operation, the NACA 65_1-208 airfoil collects less water than the NACA 65_1-212 airfoil. The extent of impingement on the upper surface of the 65_1-208 airfoil is much less than on the upper surface of the 65_1-212 airfoil, but on the lower surface the extents of impingement are about the same.

INTRODUCTION

As part of a comprehensive research program directed toward an appraisal of the problem of ice prevention on high-speed aircraft, an

investigation of the impingement of cloud droplets on airfoils and other aerodynamic bodies has been undertaken at the NACA Lewis laboratory. The investigation includes a study of the extent of impingement on low-drag airfoils and the rate of droplet impingement per unit area of the airfoil surface affected. Previous investigators have calculated the water-droplet trajectories for cylinders (refs. 1 to 6) and for Joukowski airfoils (refs. 7 and 8). An empirical method for determining area, rate, and distribution of water-droplet impingement on airfoils of arbitrary sections is presented in reference 9. The method is more firmly established for 15-percent-thick airfoils resembling Joukowski airfoil sections than for low-drag airfoils, because the basic data used in developing the empirical method were obtained for four Joukowski airfoil sections but for only one low-drag section. Some impingement data for an NACA 65_1-212 airfoil, which is a 12-percent-thick low-drag section, are presented in reference 10. Recent developments in high-speed aircraft necessitate further water-droplet trajectory studies on low-drag airfoils, particularly for thin sections, in order to determine the effect of thickness ratio on droplet impingement.

The studies presented in this report are for 8-percent- and 12-percent-thick wings designated as NACA 65_1-208 and 65_1-212 airfoils, respectively, each placed at an angle of attack of 4°. The results presented are applicable to the NACA 65_1-208 airfoil and the NACA 65_1-212 airfoil under the following conditions: chord lengths from 2 to 20 feet; altitudes from 1000 to 35,000 feet; airplane speeds from 150 miles per hour to the flight critical Mach number; droplet diameters from 5 to 100 microns; and an angle of attack of 4°. The flight critical Mach number is defined as the lowest flight speed which results in sonic velocity at some location on the airfoil.

SYMBOLS

The following symbols are used in this report:

a	droplet radius, ft
C_D	drag coefficient for droplets
C_p	pressure coefficient
d	droplet diameter, microns (micron = 3.28×10^{-6} ft)
K	inertia parameter, $\frac{2}{9}\frac{\rho_w a^2 V}{\mu L}$, dimensionless
L	airfoil chord length, ft

M	free-stream Mach number
p	absolute pressure, in. Hg
Re	local Reynolds number with respect to droplet, $2a\rho_a\bar{v}/\mu$, dimensionless
Re_0	free-stream Reynolds number with respect to droplet, $2a\rho_aV/\mu$, dimensionless
r	distance from element of vortex sheet to point in flow field, ratio to chord length
S	distance on surface of airfoil measured from leading-edge chord point, ratio to chord length
T_a	most probable icing temperature (fig. 15), ^oR
t	time, sec
U	flight speed, mph
u	local air velocity, ratio to free-stream velocity
V	free-stream velocity, ft/sec
v	local droplet velocity, ratio to free-stream velocity
$\bar{v}$	magnitude of local vector difference between velocity of droplet and velocity of air, ft/sec
W	rate of water impingement per unit span of airfoil, lb/(hr)(ft span)
W_β	local rate of water impingement, lb/(hr)(sq ft)
w	liquid-water content in cloud, g/cu m
x,y	rectangular coordinates, ratio to chord length
α	angle of attack, deg
β	local impingement efficiency, dimensionless
Γ	vortex strength, dimensionless
γ	ratio of specific heats, 1.4
μ	viscosity of air, slug/(ft)(sec)

ξ, η coordinate points on airfoil, ratio to chord length

ρ density, slug/cu ft

τ time scale, tV/L, dimensionless

Subscripts:

a air

l lower airfoil surface

m maximum

s airfoil surface

u upper airfoil surface

v vortex

w water

x horizontal component

y vertical component

0 free stream

Prime superscripts refer to coordinate system coincident with geometric chord line

ANALYSIS

As an airfoil moves through a cloud, the interception of the cloud droplets by the airfoil is dependent on the physical configuration of the airfoil, the flight conditions, and the inertia of the cloud droplets. In order to obtain the extent of impingement and the rate per unit area of droplet impingement on an airfoil, the cloud-droplet trajectories with respect to the airfoil must be determined. The differential equations that describe the droplet motion in a two-dimensional flow field have been derived in reference 4 and are presented herein in the following form:

$$\left.\begin{aligned} \frac{dv_x}{d\tau} &= \frac{C_D Re}{24} \frac{1}{K} (u_x - v_x) \\ \frac{dv_y}{d\tau} &= \frac{C_D Re}{24} \frac{1}{K} (u_y - v_y) \end{aligned}\right\} \qquad (1)$$

where

$$K \equiv \frac{2}{9} \frac{\rho_w a^2 V}{\mu L} \tag{2}$$

and the Reynolds number Re is obtained in terms of the free-stream Reynolds number so that

$$\left(\frac{Re}{Re_0}\right)^2 = (u_x - v_x)^2 + (u_y - v_y)^2 \tag{3}$$

The differential equations (1) state that the motion of a droplet is governed by the drag forces imposed on the droplet by the relative motion between the droplet and the air moving along the streamlines around the airfoil. The droplet momentum tends to keep the droplet moving in a straight path, while the drag forces tend to force the droplet to follow the streamlines. For very small droplets and low speeds, the drag forces are much greater than the inertia forces and little departure from the streamlines occurs; whereas, for large droplets and high speeds, the inertia forces tend to overcome the drag forces and the droplets depart considerably from the streamlines and follow a path more nearly in the direction established by the free-stream velocity. In accordance with equations (1) and the definition of the parameter K in equation (2), for a given size and configuration of airfoil the trajectories depend on the radius of the droplets, the airspeed, and the air viscosity as first-order variables. The trajectories also depend on the geometry of the airfoil involved and its angle of attack, in that these two variables determine the magnitude of the component velocities of the air u_x and u_y everywhere in the flow field.

The component air velocities were determined by a vortex substitution method that requires a knowledge of the pressure distribution on the surface of the airfoil. The pressure distribution was obtained from wind-tunnel data taken at the NACA Ames laboratory. The fundamentals of the method for calculating the local perturbation velocities in a two-dimensional incompressible flow field ahead of an airfoil are established in reference 11. The procedure for the calculations is presented in appendix A. The computations were performed with electronic calculating machines employing punched cards. Although the compressibility of air at high speeds is not accounted for with the vortex substitution method, results presented in reference 5 show that the effect of the compressibility of air on the trajectories of droplets is negligible up to the critical Mach number of the airfoil. Because of these studies, the results presented herein are considered applicable up to the flight critical Mach number.

Assumptions that have been necessary in order to solve the problem are:

(1) At a large distance ahead of the airfoil (free-stream conditions) the droplets do not move with respect to the air.

(2) No gravitational force acts on the droplets.

(3) The droplets are always spherical and do not change in size.

The first two assumptions are valid for droplets smaller than drizzle or rain drops, because the inertial forces of the drops are much greater than the gravitational force. The assumptions are usually also valid for falling rain drops, since the airplane velocity is usually much greater than the drop velocity caused by gravitational force. Preliminary calculations show that the third assumption is valid for the order of accuracy usually required in the design of equipment for the protection of aircraft.

METHOD OF SOLUTION

The differential equations of motion (eq. (1)) are difficult to solve by ordinary means, because the values of the velocity components of the air and the term containing the coefficient of drag are not known until the trajectory is traced. These values are determined as the trajectory of a droplet is developed, since the magnitudes depend on the position of the droplet in the flow field. Simultaneous solutions for the two equations were obtained with a mechanical analog constructed at the Lewis laboratory for this purpose. The answers were obtained in the form of plots of the droplet trajectories with respect to the airfoil. The coefficient of drag C_D for the droplets, required in equations (1), was obtained from tables in reference 3.

The equations of motion (eq. (1)) were solved for the following five values of the parameter K: 1/100, 1/50, 1/10, 1/5, and 1. For each value of the parameter K, a series of trajectories was computed for each of three values of free-stream Reynolds number Re_0: 16, 256, and 1024 (where necessary, $Re_0 = 64$ was also computed). (A graphical procedure for translating the dimensionless parameters used in this report into terms of airplane speed, chord length, altitude, and droplet size is presented in appendix B.) Each series of trajectories encompassed the airfoil with a trajectory that was tangent to the upper surface of the airfoil and with a trajectory that was tangent to the lower surface of the airfoil. The upper and lower tangent trajectories started at free-stream conditions at distances $y_{0,u}$ and $y_{0,l}$, respectively, from the x-axis of the rectangular coordinate system (fig. 1). The geometric chord line

of the airfoil is oriented at an angle of 4° with the x-axis of the rectangular coordinate system, and the leading edge is placed at the origin of the coordinates. At an infinite distance ahead of the airfoil, the uniform air flow carrying the cloud droplets is assumed to be approaching the airfoil from the negative x-direction, and parallel to the x-axis. All distances are dimensionless, because they are ratios to the airfoil chord length L, which is the unit of distance.

Before the integration of the equations of motion could be performed with the analog, the initial velocity of the droplets had to be determined. As postulated in the assumptions, at an infinite distance ahead of the airfoil all the droplets have vertical and horizontal components of velocity relative to the airfoil that are the same as those of the free-stream air. At finite distances ahead of the leading edge of the airfoil, the droplets have velocity components varying between those pertaining to the free stream at infinity and those pertaining to the local streamlines. At 5 chord lengths ahead of the airfoil, the air streamlines deviated from free-stream conditions by less than the expected accuracy of the analog; therefore, this point was assumed to be sufficiently ahead of the airfoil so that the velocity components of the air streamlines could be assigned to the droplets. Since the time required to trace each trajectory from 5 chord lengths ahead of the airfoil to the airfoil surface was prohibitive, plotting by the analog was started at 1 chord length ahead of the airfoil leading edge. The starting conditions at this point were determined by calculating a sample trajectory that started at $x = -5$ for each of the five values of K studied. A preliminary study showed that while a droplet is approaching a position 1 chord length ahead of the airfoil, the amount of deviation of the droplet trajectory from the air streamline on which the droplet had started depends only on the value of K and not on the starting value of y at $x = -5$, nor on the value of Re_0, provided the values of y and Re_0 are within the region of interest in the problem. The sample trajectories for each value of K studied were calculated from $x = -5$ to $x = -1$ in order to determine the starting values of droplet velocity and y-ordinate at $x = -1$; thus, the final results were the same as if each trajectory were calculated from 5 chord lengths ahead of the airfoil leading edge.

RESULTS AND DISCUSSION

The series of trajectories computed for each combination of values of K and Re_0 studied permits evaluation of the area, the rate, and the distribution of water-droplet impingement on the NACA 65_1-208 and the NACA 65_1-212 airfoil sections at an angle of attack of 4°. The amount of water collected and the area, or extent, of impingement are determined by

the limiting trajectories, which are tangent to the airfoil. All droplets having trajectories between the tangent trajectories will strike the airfoil, whereas all other droplets will miss the airfoil. The tangent trajectories determine the maximum, or total, rate of droplet impingement, because the amount of water-droplet impingement on the whole wing is governed by the spacing between the tangent trajectories ($y_{0,u} - y_{0,l}$, fig. 1) at a large distance ahead of the airfoil. The manner in which all the droplets collected on the surface are distributed over the area of impingement is determined by the behavior of the intermediate trajectories that are bounded by the tangent trajectories.

The results are often presented herein as functions of the parameter K, which has been called the inertia parameter because its magnitude directly reflects the external force required on a droplet to cause a deviation from its original line of motion. For large values of K (i.e., $K>1$), which correspond, for example, to droplets larger than 50 microns in diameter moving toward a 5-foot-chord airfoil at 400 miles per hour, the droplet trajectories deviate by only small amounts from straight lines. For values of K less than 1/50, which correspond, for example, to droplets less than 12 microns in diameter moving at less than 300 miles per hour toward an airfoil section with a 12-foot chord, the droplet trajectories more nearly coincide with the air streamlines.

Rate of Water Interception

In flight, the rate of total water interception (lb/(hr)(ft span)) is determined by both the tangent droplet trajectories and the liquid-water content in the cloud. The airfoil speed, the size of the airfoil, and the droplet size are the principal variables affecting the tangent droplet trajectories. The spacing between the upper and lower tangent trajectories, which is a measure of the rate of total water interception, is given in figure 2 for both the 65_1-208 and the 65_1-212 airfoils. The rate of total water interception per unit span of airfoil on that portion of the airfoil surface bounded by the upper and the lower tangent trajectories (fig. 1) can be calculated from the information in figure 2 and the following relation:

$$W_m = 0.329(y_{0,u} - y_{0,l})\,LUw \qquad (5)$$

where the flight speed U is in miles per hour and the liquid-water content w is in grams per cubic meter.

For both airfoils, the rate of water interception is decreased as $1/K$ is increased, particularly for values of $1/K$ larger than 1. An increase in Re_0 decreases slightly the rate of water interception. The following example illustrates the use of figure 2 and equation (5)

in comparing the two airfoils in terms of conventional flight units. The values of $1/K = 21$ and $Re_0 = 171$ represent the conditions for airfoils with 12-foot chords traveling at 400 miles per hour through a cloud composed of droplets 17 microns in diameter at an altitude of 10,000 feet ($1/K$ and Re_0 based on most probable icing temperature, appendix B). The corresponding value for $(y_{0,u} - y_{0,l})$ required for equation (5) is 0.017 for a 65_1-208 airfoil as compared with 0.021 for a 65_1-212 airfoil. If the same airfoils are considered in flight at 200 miles per hour (droplet size, liquid-water content, and altitude not varied), the values of $1/K$ and Re_0 change to 42 and 85, respectively, and the value of $(y_{0,u} - y_{0,l})$ changes to 0.013 for the 8-percent-thick airfoil and to 0.015 for the 12-percent-thick airfoil, a decrease of 24 and 28 percent, respectively, from the corresponding values associated with flight at 400 miles per hour. The decrease in rate of water impingement (eq. (5)) is 62 percent for the 8-percent-thick airfoil and 64 percent for the 12-percent-thick airfoil. The effect of speed on the rate of water impingement is large, because the spacing between the two tangent trajectories increases with the increase in flight speed and the speed also appears directly in equation (5).

2762

The rate of water interception is less on the 8-percent-thick airfoil than on the 12-percent-thick airfoil over the complete range of free-stream Reynolds number and inertia parameter studied (flight speed, altitude, droplet sizes encountered in clouds, and airfoil size) except for combinations of $1/K > 65$ and $Re_0 < 32$, which correspond, for example, to flight with an airfoil chord length larger than 5 feet at a speed of less than 150 miles per hour through clouds at 15,000 feet altitude composed of droplets less than 10 microns in diameter.

CN-2

The variation of rate of water interception with airfoil speed is summarized for an altitude of 20,000 feet in figure 3, in which the ordinate W_m/w is the total rate of water impingement per foot span of airfoil per unit liquid-water content (g/cu m) in the cloud. (Fig. 3 is based on most probable icing temperature, appendix B). The total rate of water impingement can be obtained as a product of the results in figure 3 and the liquid-water content existing in the cloud. The values in figure 3 are for flight through a uniform cloud composed of droplets 15, 20, 30, and 40 microns in diameter, with several chord lengths ranging in value from 2 to 20 feet considered.

The effect of altitude on the rate of water impingement is shown in figure 4 for droplets smaller than 40 microns in diameter. The values for rate of water impingement given in figure 3 can be corrected to a first order of approximation for the altitude effect with the use of figure 4. For example, the rates of water impingement given in figure 3(c) can be corrected for use at 10,000 feet altitude by reducing the values

of rate of water impingement given in figure 3(c) by 7 percent, because for 30-micron droplets the rate of water impingement at 10,000 feet is approximately 7 percent less than at 20,000 feet (fig. 4). A change in altitude of 10,000 feet for any given droplet size shown in figure 4 does not produce as large an effect on the rate of water impingement as does a 15-percent change in droplet size at a given altitude. The effect of moderate changes in altitude may be ignored, because the droplet size and the liquid-water content of clouds are seldom known with sufficient accuracy to permit the rate of water collection to be calculated within 10 percent. Therefore, within the practical limits of application, the results of figure 3 can be used over a wide range of altitudes.

The effect of wing taper on the rate of water impingement, as can be obtained from the results in figure 3, is valid, provided that for each section of span considered the taper is small enough to permit the approximation of two-dimensional flow over the section. For a 65_1-208 airfoil section with a 14-foot chord at the root section and a 4-foot chord at the tip section moving at 400 miles an hour at an altitude of 20,000 feet through a cloud composed of droplets 20 microns in diameter and containing a liquid-water content of 1 gram per cubic meter, the rate of total water impingement is 35 pounds per hour per foot span at the root section and 17 pounds per hour per foot span at the tip section. A 12-percent-thick airfoil of the same size and section subjected to the same flight and atmospheric conditions as given for the 8-percent-thick airfoil collects approximately 28 percent more water at both the root and tip sections.

Extent of Impingement

A knowledge of the chordwise extent of impingement on the upper and lower wing surfaces is necessary for the design of anti-icing equipment. The limit of impingement is determined by the point of tangency on the airfoil of the tangent trajectories. The rearward limits of impingement on the upper surface are shown in figure 5(a), and those on the lower surface, in figure 5(b). The distances S_u and S_l are measured on the surface from the point of intersection of the geometric chord line with the leading edge (fig. 1) in terms of the chord length.

The limit of impingement on the 65_1-208 airfoil is compared in figure 5 with that on a 65_1-212 airfoil. The impingement extends much farther back over the top surface of the 12-percent-thick airfoil than over the top surface of the 8-percent-thick airfoil (fig. 5(a)). The impingement extends farther back along the bottom surface of the thicker airfoil over most flight and atmospheric conditions, but is farther back on the lower surface of the 8-percent-thick airfoil for combinations of flight and atmospheric conditions involving $1/K$ values smaller than 1.5 and larger than 50.

The rearward limit of impingement along the upper and lower surfaces, respectively, is summarized in figures 6 and 7 for the same speeds, chord lengths, droplet sizes, and altitude as given in figure 3. The extent of impingement on both the upper and lower surfaces increases with increasing speed and with decreasing chord length. It is much greater along the lower surface than along the upper surface. As an example, for the 65_1-208 airfoil with a 14-foot chord traveling at 300 miles per hour through a cloud composed of droplets 20 microns in diameter, the extent of impingement on the upper surface is 0.006 chord (fig. 6(b)), and on the lower surface is 0.071 chord (fig. 7(b)). Again, as shown in figure 5, the extent of impingement on the 8-percent-thick airfoil is less than on the 12-percent-thick airfoil, except on the lower surface for combinations of low flight speed and large chord length and, particularly, with the smaller droplets considered in figure 7(a). These combinations of low flight speeds and large chord lengths given in figure 7(a) correspond to conditions involving values of $1/K$ larger than 50 shown in figure 5(b). The combination of conditions involving values of $1/K<1.5$, for which the extent of impingement on the lower surface of the 8-percent-thick airfoil is also greater than on the lower surface of the 12-percent-thick airfoil, is given in figure 7(c) and 7(d). Values of $1/K<1.5$ are involved, for example, with combinations of airfoil chord lengths smaller than 4 feet and flight speeds greater than 400 miles per hour for a droplet size of 40 microns, as shown in figure 7(d).

Impingement Distribution Along Airfoil Surface

In the design of thermal anti-icing systems based either on the principle of maintaining the water in the liquid state or of completely evaporating the impinging water, a knowledge of the distribution of the water impingement along the airfoil surface is required. The distribution can be obtained if the starting ordinate y_0 at infinity of a droplet trajectory is known with respect to the point of impingement on the surface. The starting and ending positions of the trajectories are shown in figure 8 for the three values of free-stream Reynolds number studied. For each value of Re_0, curves for several values of $1/K$ are given.

The amount of water impinging between any two given points on the airfoil surface may be found by applying the results given in figure 8 in the relation

$$W = 0.329UwL(y_{0,1} - y_{0,2}) \qquad (8)$$

For example, the amount of water impinging between the -0.05-chord point and the -0.10-chord point on the surface of a 12.5-foot-chord airfoil

moving at 400 miles per hour at an altitude of 10,000 feet through a cloud composed of droplets 25 microns in diameter ($1/K = 10$, $Re_0 \simeq 256$) is determined by obtaining the values of $y_{0,2}$ at the -0.10-chord point and $y_{0,1}$ at the -0.05-chord point. The values of $y_{0,1}$ and $y_{0,2}$ required in equation (8) are -0.074 and -0.078 for the 8-percent-thick airfoil and -0.071 and -0.076 for the 12-percent-thick airfoil, respectively (fig. 8).

The values of $(y_{0,u} - y_{0,l})$, obtained from the end points of each curve in figure 8, are the same as the values given in figure 2. The values of $y_{0,l}$ for $1/K = 0$ (not shown in fig. 8) are -0.0644 at $S = -0.654$ chord for the 8-percent-thick airfoil and -0.0825 at $S = -0.538$ chord for the 12-percent-thick airfoil. These values for $1/K = 0$ apply for all values of free-stream Reynolds number Re_0.

Local Rate of Droplet Impingement

The local rate of droplet impingement per unit area of airfoil surface can be determined from the expression

$$W_\beta = 0.329Uw \frac{dy_0}{dS} = 0.329Uw\beta \qquad (9)$$

This equation is related to equation (8), with proper considerations for the fact that y_0 and S are based on the wing chord L. The values of the local impingement efficiency β as a function of the airfoil distance S are given in figures 9 and 10. These values were obtained from the slopes of the curves in figure 8. The values of β for the NACA 65_1-208 airfoil are given in figure 9, and for the 65_1-212 airfoil, in figure 10. For both airfoils, the maximum rate of local impingement occurs between the air stagnation line and the leading edge. The air stagnation line is located at $S_l = 0.013$ on the 65_1-208 airfoil and at $S_l = 0.008$ on the 65_1-212 airfoil (at 4° angle of attack).

Because of the geometry of the airfoil and the manner in which the droplets approach the airfoils in the neighborhood of the stagnation line and the leading-edge line, the curves in figure 8 are not all well defined between $S = -0.01$ and $S = 0$. Since the values of β are obtained from the slopes of the curves in figure 8, the maximum values of β in figures 9 and 10 also are subject to some question. The possible error in the maximum value of β is estimated to be ± 20 percent for the curves in figure 9 and ± 15 percent for the curves in figure 10. The difference in the possible error is due to the difference in the bluntness of the two

airfoils. This possible error is not considered very serious, because only a small portion of the total water impinging on the airfoil requires redistribution if the maximum value of β is changed by as much as the maximum possible error. The total area under the curves should not be changed when a change in the maximum value of β is made, because the total amount of water impinging, determined by $(y_{0,u} - y_{0,l})$ and by $\int_{S_l}^{S_u} \beta \, dS$, is independent of the manner in which the water is distributed near the leading edge. Any judicious refairing of the curves in figures 9 and 10 between $S = -0.01$ and $S = 0$, which is the region of doubt, to account for as much as the largest possible error in the maximum value of β will rearrange only a small area under the present curves (total area must not be changed) and thus affect the redistribution of only a small amount of the total water.

The maximum local rate of impingement shown for these airfoils in figures 9 and 10 coincides very nearly with the location of the parting strip recommended in references 12 and 13 for use in cyclical thermal de-icing systems.

CONCLUDING REMARKS

The data presented in figures 2 to 10 apply directly to flights in clouds composed of droplets that are all uniform in size. The water droplets in a cloud, however, are not necessarily uniform in size; the extent of impingement is always determined by the largest droplets present in sufficient number to represent a significant portion of the total water present in the cloud. The local rates of droplet impingement are also determined by the droplet-size distribution patterns present in the cloud. For flights in clouds composed of droplets that are not uniform in size, the β curves of figures 9 and 10 must be altered to conform with the weighted basis of the droplet-size distribution. A detailed procedure for weighting the impingement of droplets existing in nonuniform clouds is presented in reference 4.

The data presented in this report apply directly to nonswept wings of high aspect ratio. As previously stated, the data also apply to wings with small amounts of taper. A method for extending the impingement calculations for nonswept wings to swept wings is presented in reference 14. The method presented in reference 14 permits the application of the data presented herein to a wing with any angle of yaw provided the airfoil section normal to the leading edge is an NACA 65_1-208 or an NACA

65_1-212 airfoil. If the airfoil section on the aircraft under consideration is laid out parallel to the free-stream direction, a transformation of the section is necessary, as described in reference 14.

Lewis Flight Propulsion Laboratory
National Advisory Committee for Aeronautics
Cleveland, Ohio, January 30, 1953

APPENDIX A

METHOD USED TO CALCULATE INCOMPRESSIBLE FLOW FIELD AROUND AIRFOIL

The velocities in the two-dimensional flow field were calculated by distributing a sheet of vortices on the airfoil surface of such strength that the velocities on the surface caused by the vortices were the same as the velocities measured in a wind tunnel. The principles upon which this method is based are established in reference 11.

The velocity at the surface of an airfoil can be determined from a knowledge of the pressure coefficient C_p and the free-stream Mach number M with the aid of the following expression:

$$u_s = \sqrt{1 + \frac{2}{(\gamma - 1)M^2}\left[1 - \left(\frac{C_p \gamma M + 2}{2}\right)^{\frac{\gamma-1}{\gamma}}\right]} \qquad (A1)$$

The pressure coefficients for a large number of points on the surface of the NACA 65_1-208 and 65_1-212 airfoils at an angle of attack of 4° were obtained from wind-tunnel data taken at the NACA Ames laboratory for several free-stream Mach numbers. The surface velocities used to calculate the flow field are shown in figure 11 for a Mach number of 0.2. The flow fields at other Mach numbers were not calculated, because the results presented in reference 5 show that the effect of the compressibility of the air on the droplet trajectories is negligible.

The velocity at a point in a flow field caused by an element of the vortex sheet of strength $\Delta\Gamma$ placed a distance r (fig. 12) from the point is

$$u_v = \frac{\Delta\Gamma}{2\pi r}$$

If an element of vortex sheet of strength

$$\Delta\Gamma_i \equiv (u_s \Delta S)_i$$

is placed on an increment ΔS of the airfoil at the i^{th} position on the airfoil surface, the velocity caused only by the i^{th} section of the airfoil is

$$u_v = \frac{(u_s \Delta S)_i}{2\pi r_i}$$

at a point in the flow field at a distance r_i from the i^{th} section (fig. 12). The local components of the perturbation velocity, at a point in the flow field, caused by 300 vortex elements distributed on both the upper and lower surfaces of the airfoil are

$$\left.\begin{aligned} u_{x',v} &= \sum_{i=0}^{300} \frac{u_s}{2\pi} \frac{y'-\eta}{r^2} \Delta S \\ u_{y',v} &= \sum_{i=0}^{300} \frac{u_s}{2\pi} \frac{\xi-x'}{r^2} \Delta S \end{aligned}\right\} \qquad \text{(A2)}$$

The coordinate system shown in figure 12 differs from that shown in figure 1, in that in figure 12 one of the coordinates coincides with the geometric chord line. The direction of the free-stream velocity is toward the airfoil at an angle α with respect to $-x'$. The horizontal and vertical components of the local velocity $u_{x'}$ and $u_{y'}$, respectively, are obtained by adding $V \cos \alpha$ to $u_{x',v}$ and $V \sin \alpha$ to $u_{y',v}$. The coordinate system shown in figure 12 was used because of its adaptability to available calculating equipment and procedures. The trajectories were solved in the primed coordinate system shown in figure 12 and later transformed graphically to the system presented in figure 1.

A total of 300 vortex elements were used on the airfoil with a much denser distribution on the forward section than beyond the 50-percent-chord point. Equations (A2) were solved with electronic calculating machines. Approximately 300 points were computed in the flow field out to 1 chord length ahead of the airfoil in the region of interest with regard to computing the trajectories of droplets that strike the airfoil. Between 1 and 5 chord lengths ahead of the airfoil leading edge, the flow-field velocity components were approximated by assuming that the flow was caused by a single vortex located on the airfoil chord line 25-percent chord inward from the leading edge. The strength of this vortex was determined by the requirement that at $x' = -1$ the vertical velocity caused by this single vortex must be the same as that computed with equation (A2).

APPENDIX B

GRAPHICAL PROCEDURE FOR TRANSLATION OF PRACTICAL FLIGHT CONDITIONS IN TERMS OF DIMENSIONLESS PARAMETERS

A graphical procedure is presented to aid in the translation of airplane speed, chord size, altitude, and droplet diameter into terms of the dimensionless parameters K and Re_0 used in this report. A solution of equation (2) is presented in figure 13 for two altitudes. For given droplet diameters in microns and ratios of the chord length in feet to the flight speed in miles per hour, the reciprocal of the inertia parameter can be determined at altitudes of either 10,000 or 30,000 feet from figure 13. Altitude does not appreciably affect the value of $1/K$, as can be noted from a comparison of values in figure 13(a) with those in figure 13(b).

An airfoil with a 12-foot chord length at a flight speed of 400 miles per hour and an altitude of 10,000 feet passing through a cloud composed of droplets all of which are 17 microns in diameter will be used as an example in the graphical procedure to interpret practical flight units into terms of the dimensionless parameters. The value of $1/K$ is obtained from figure 13(a) for the value of $\frac{L}{U} = \frac{12}{400} = 0.0300$ and droplet diameter $d = 17$. The value of $1/K$ obtained from figure 13(a) is 21.

The free-stream Reynolds number for different altitudes may be obtained from figure 14. The product of the droplet diameter in microns and the flight speed in miles per hour must be known. The Reynolds number is a function of the air density, which depends on the pressure and the temperature at the altitudes considered. The pressure used to calculate the air density was taken from tables of NACA standard atmospheric pressure at various altitudes, but the temperature was based on the most probable icing temperature at various altitudes. The most probable icing temperature was obtained from approximately 300 icing observations (ref. 15) and is presented in figure 15. For the example under consideration, the product of the droplet diameter and the flight speed is $(17)(400) = 6800$. The value of Re_0, obtained from figure 14, is 171.

The following relations are presented for use when the degree of accuracy required is not attainable with the graphical procedure. The values for the viscosity μ should be obtained from figure 16; these values are based on the most probable icing temperature of figure 15. The charts of figures 13 and 14 are based on the most probable icing temperature and viscosity.

$$K = 1.704 \times 10^{-12} \frac{d^2 U}{\mu L}$$

$$Re_0 = 4.813 \times 10^{-6} \frac{d \rho_a U}{\mu}$$

$$d = 7.662 \times 10^{5} \sqrt{\frac{K \mu L}{U}}$$

$$\rho_a = 0.0412 \frac{p}{T_a}$$

where the units are given in the list of symbols. (The density of water was assumed to be 62.46 lb/cu ft and the acceleration due to gravity, 32.17 ft/sec^2.)

REFERENCES

1. Glauert, Muriel: A Method of Constructing the Paths of Raindrops of Different Diameters Moving in the Neighborhood of (1) a Circular Cylinder, (2) an Aerofoil, Placed in a Uniform Stream of Air; and a Determination of the Rate of Deposit of the Drops on the Surface and the Percentage of Drops Caught. R. & M. No. 2025, British A.R.C., 1940.

2. Ranz, W. E.: The Impaction of Aerosol Particles on Cylindrical and Spherical Collectors. Tech. Rep. No. 3, Eng. Exp. Station, Univ. Ill., March 31, 1951. (Contract No. AT(30-3)-28, U.S. Atomic Energy Commission.)

3. Langmuir, Irving, and Blodgett, Katherine B.: A Mathematical Investigation of Water Droplet Trajectories. Tech. Rep. No. 5418, Air Materiel Command, AAF, Feb. 19, 1946. (Contract No. W-33-038-ac-9151 with General Electric Co.)

4. Brun, Rinaldo J., and Mergler, Harry W.: Impingement of Water Droplets on a Cylinder in an Incompressible Flow Field and Evaluation of Rotating Multicylinder Method for Measurement of Droplet-Size Distribution, Volume-Median Droplet Size, and Liquid-Water Content in Clouds. NACA TN 2904, 1953.

5. Brun, Rinaldo J., Serafini, John S., and Gallagher, Helen M.: Impingement of Cloud Droplets on Aerodynamic Bodies as Affected by the Compressibility of Air Flow Around the Body. NACA TN 2903, 1953.

6. Brun, Edmond, Caron, Robert, et Marcel, Vasseur: Introduction á l'étude de la Mécanique des Suspensions. G.R.A. Rapport Tech. No. 15, Recherches Aéronautiques (Paris), 1945.

7. Bergrun, Norman R.: A Method for Numerically Calculating the Area and Distribution of Water Impingement on the Leading Edge of an Airfoil in a Cloud. NACA TN 1397, 1947.

8. Guibert, A. G., Janssen, E., and Robbins, W. M.: Determination of Rate, Area, and Distribution of Impingement of Waterdrops on Various Airfoils from Trajectories Obtained on the Differential Analyzer. NACA RM 9A05, 1949.

9. Bergrun, Norman R.: An Emperical Method Permitting Rapid Determination of the Area, Rate, and Distribution of Water-Drop Impingement on an Airfoil of Arbitrary Section at Subsonic Speeds. NACA TN 2476, 1951.

10. Brun, Rinaldo J., Serafini, John S., and Moshos, George J.: Impingement of Water Droplets on an NACA 65_1-212 Airfoil at an Angle of Attack of 4°. NACA RM E52B12, 1952.

11. von Mises, Richard: Theory of Flight. McGraw-Hill Book Co., Inc., First ed., 1945.

12. Gray, V. H., Bowden, D. T., and von Glahn, U.: Preliminary Results of Cyclical De-icing of a Gas-Heated Airfoil. NACA RM E51J29, 1952.

13. Lewis, James P., and Bowden, Dean T.: Preliminary Investigation of Cyclic De-Icing of an Airfoil Using an External Electric Heater. NACA RM E51J30, 1952.

14. Dorsch, Robert G., and Brun, Rinaldo J.: A Method for Determining Cloud-Droplet Impingement on Swept Wings. NACA TN 2931, 1953.

15. Hacker, Paul T., and Dorsch, Robert G.: A Summary of Meteorological Conditions Associated with Aircraft Icing and a Proposed Method of Selecting Design Criterions for Ice-Prevention Equipment. NACA TN 2569, 1951.

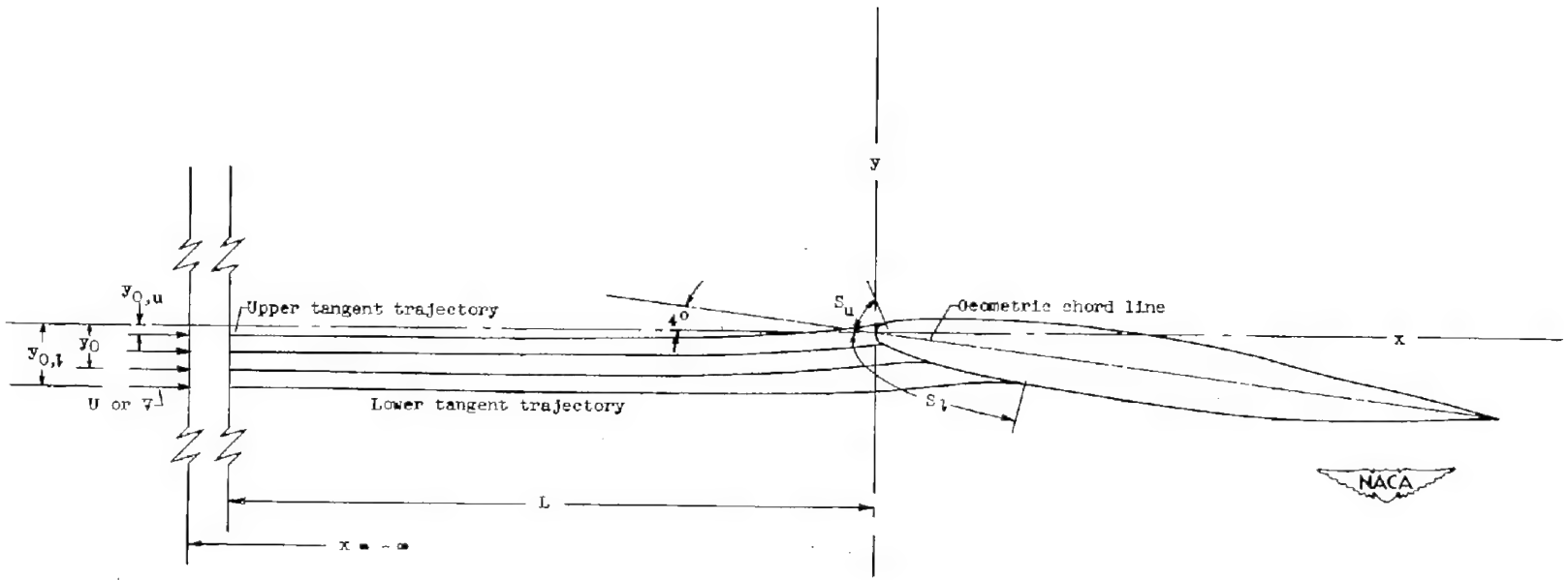

Figure 1. - Droplet trajectories with respect to airfoil.

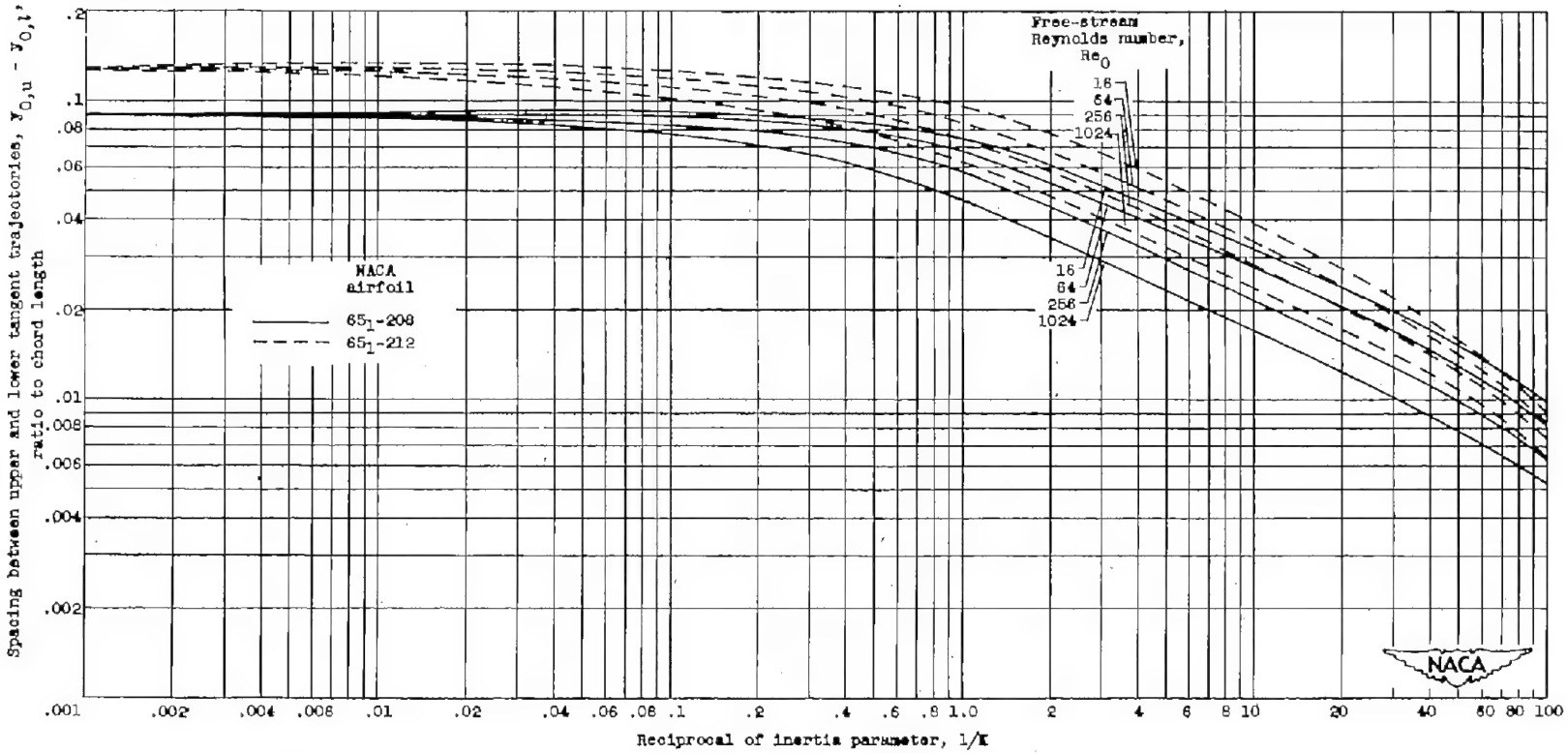

Figure 2. - Spacing between upper and lower tangent trajectories at free-stream conditions. Angle of attack, 4°.

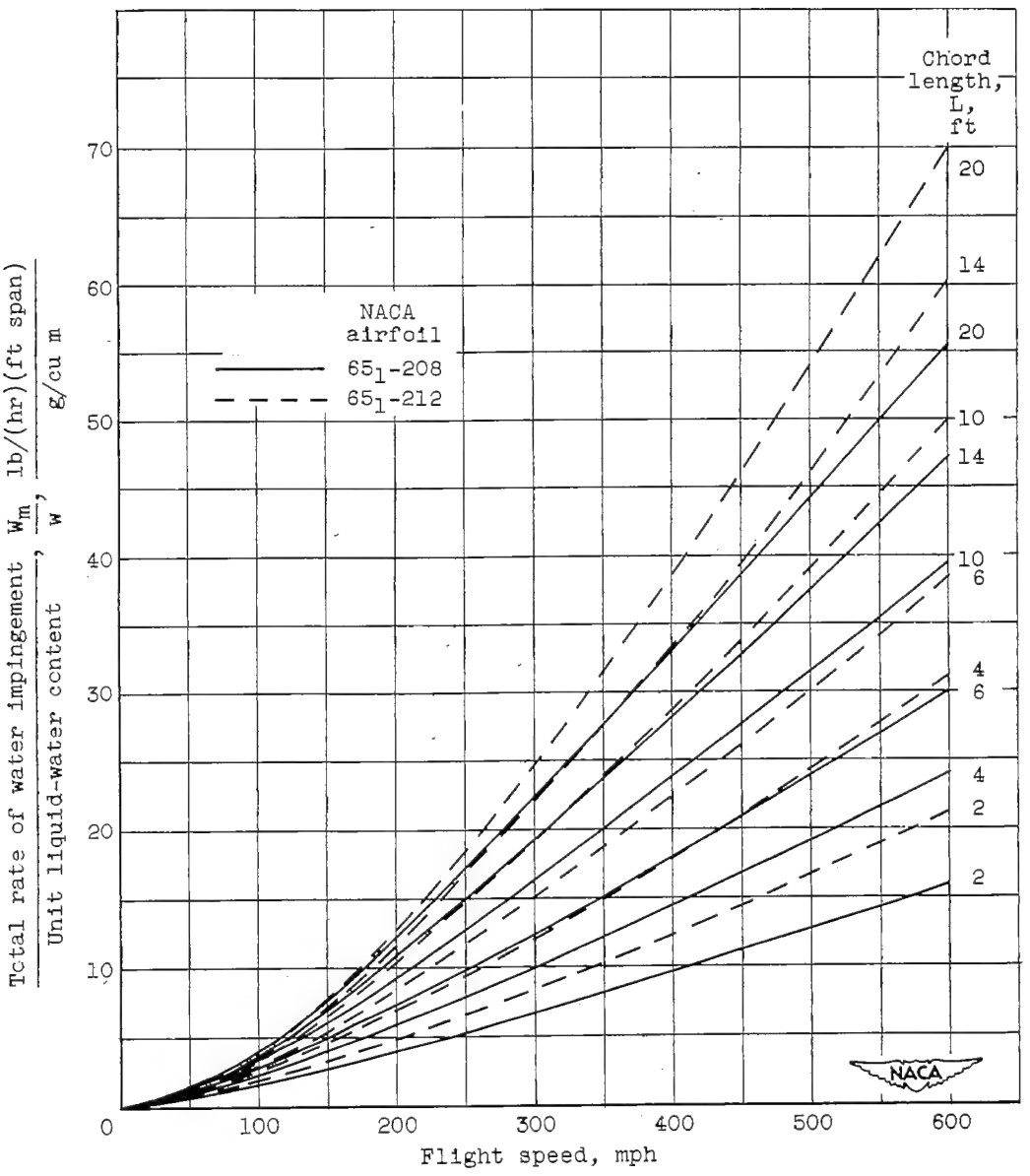

(a) Droplet size, 15 microns.

Figure 3. - Rate of water impingement. Angle of attack, 4°; altitude, 20,000 feet; most probable icing temperature, -11° F.

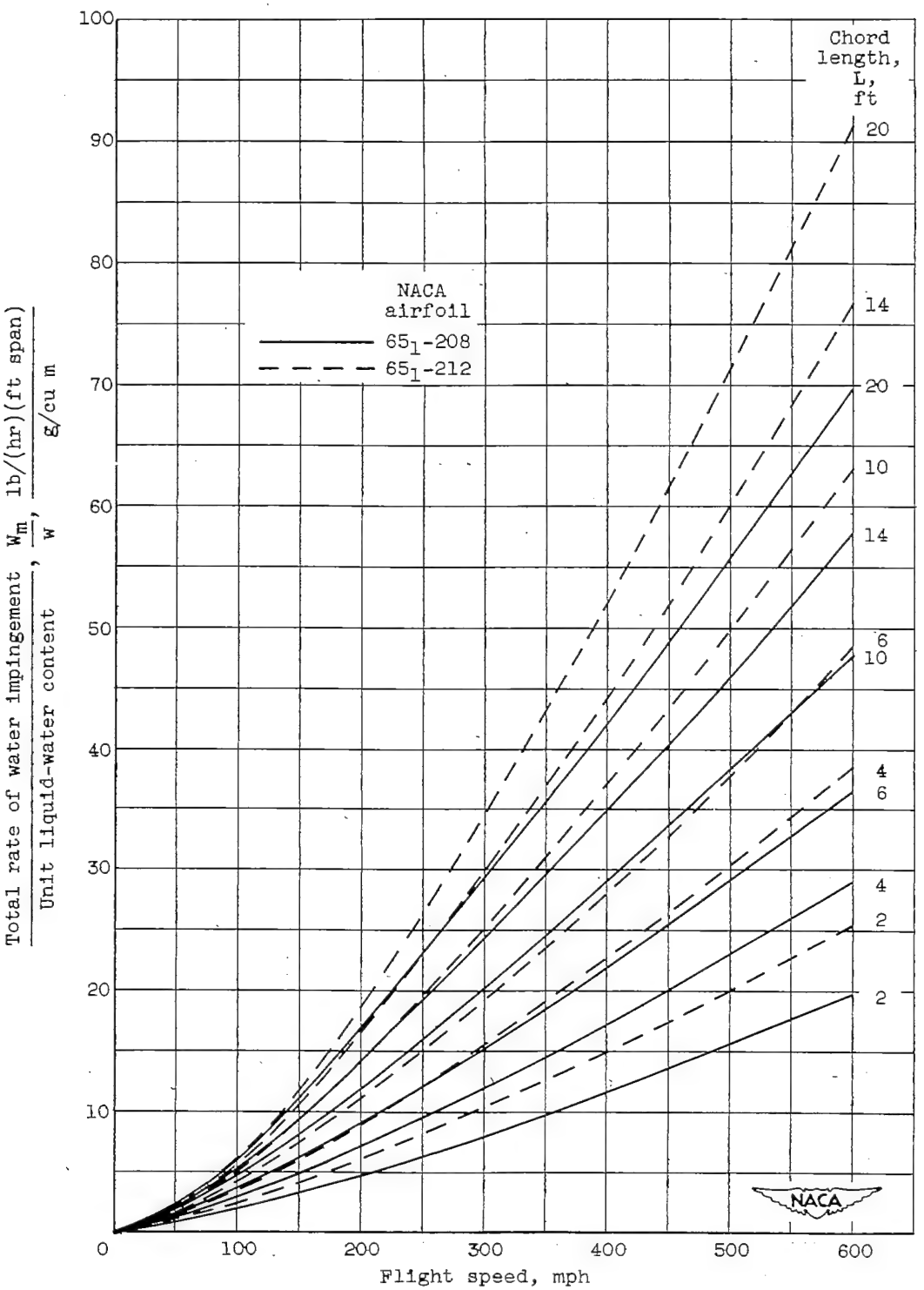

(b) Droplet size, 20 microns.

Figure 3. - Continued. Rate of water impingement. Angle of attack, 4°; altitude, 20,000 feet; most probable icing temperature, -11° F.

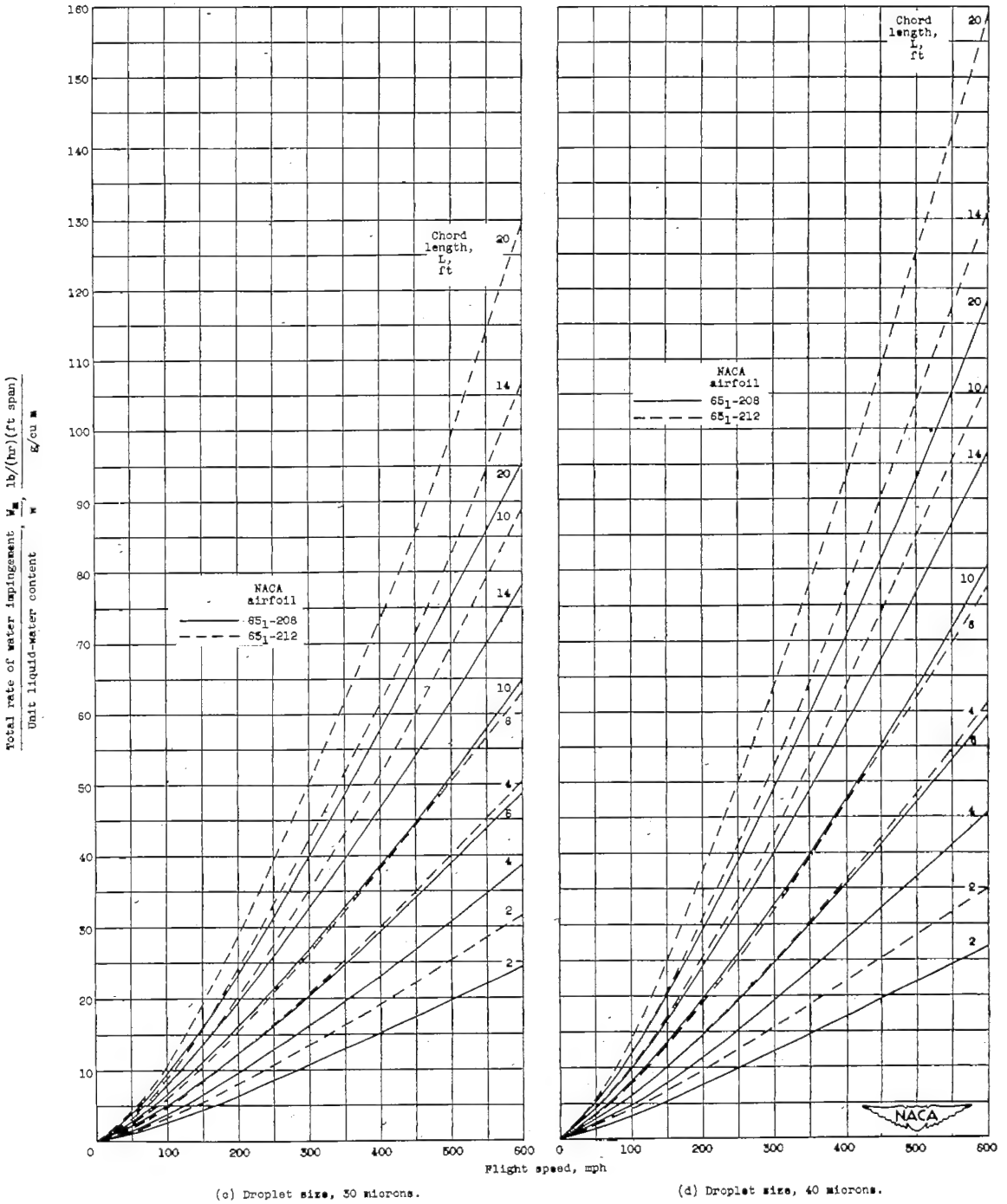

(c) Droplet size, 30 microns.

(d) Droplet size, 40 microns.

Figure 3. - Concluded. Rate of water impingement. Angle of attack, 4°; altitude, 20,000 feet; most probable icing temperature, -11° F.

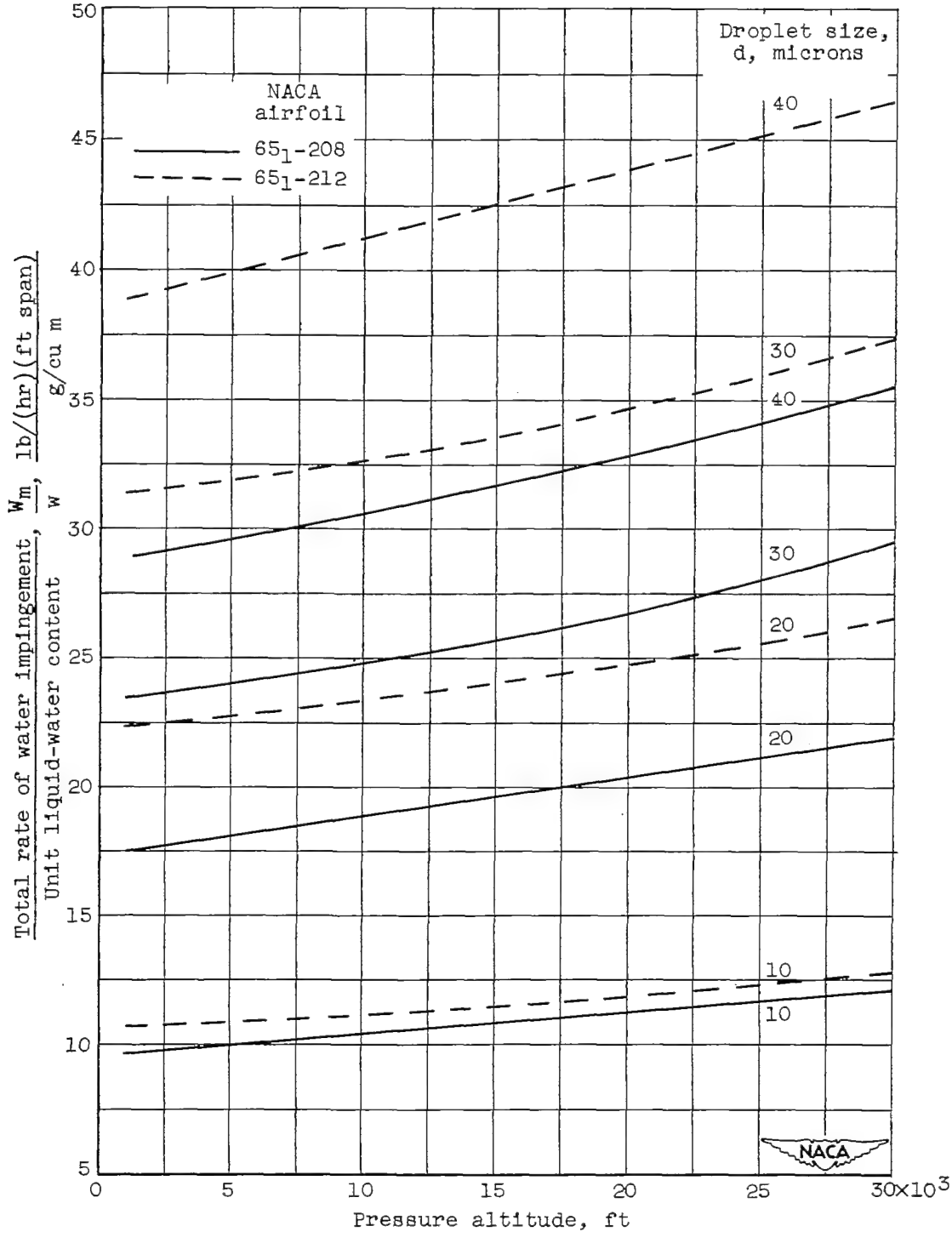

Figure 4. - Effect of altitude on rate of water impingement. Chord length, 10 feet; airplane speed, 300 miles per hour; most probable icing temperature, (see appendix B).

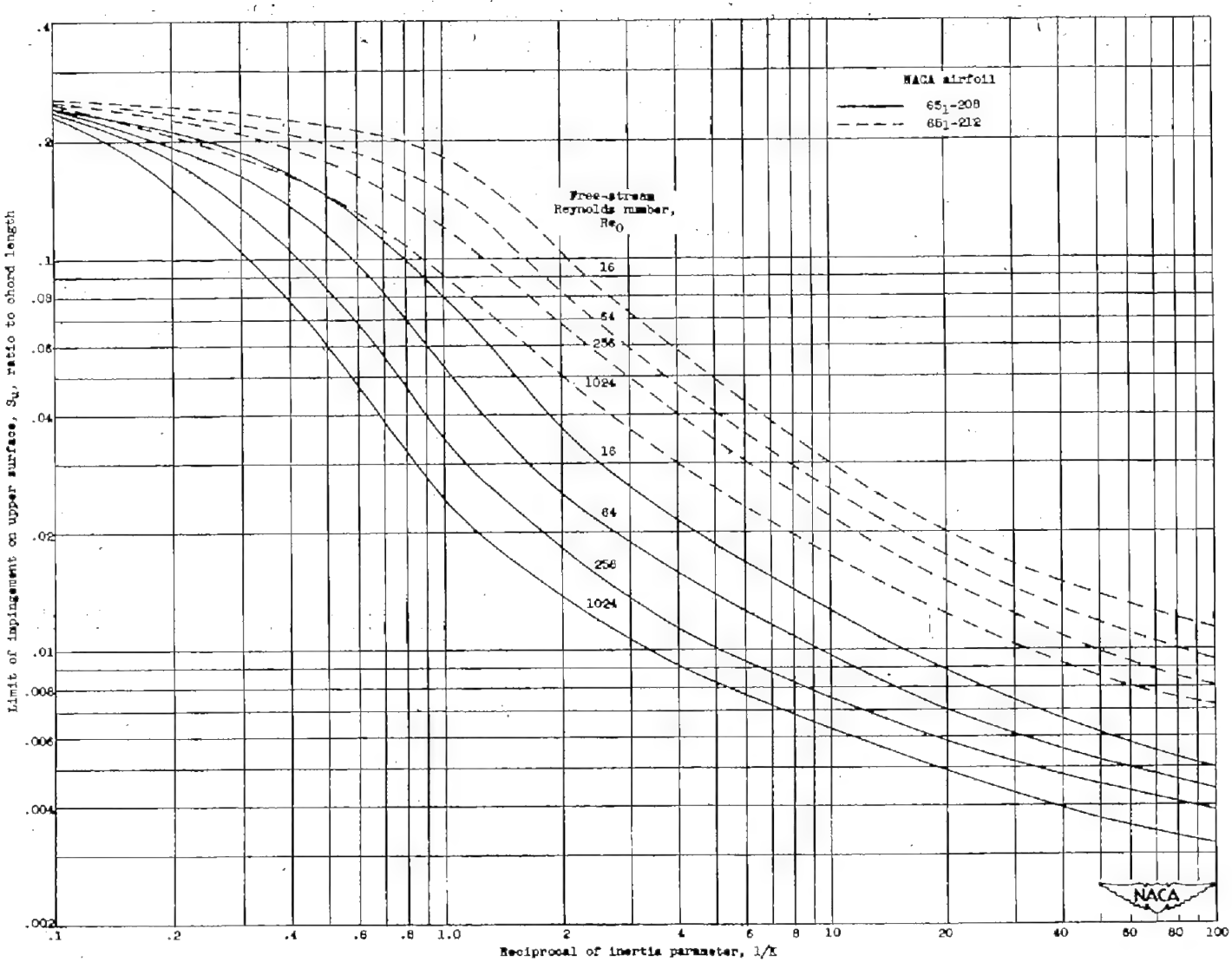

(a) Upper surface.

Figure 8. - Limit of impingement on airfoil surface. Angle of attack, 4°.

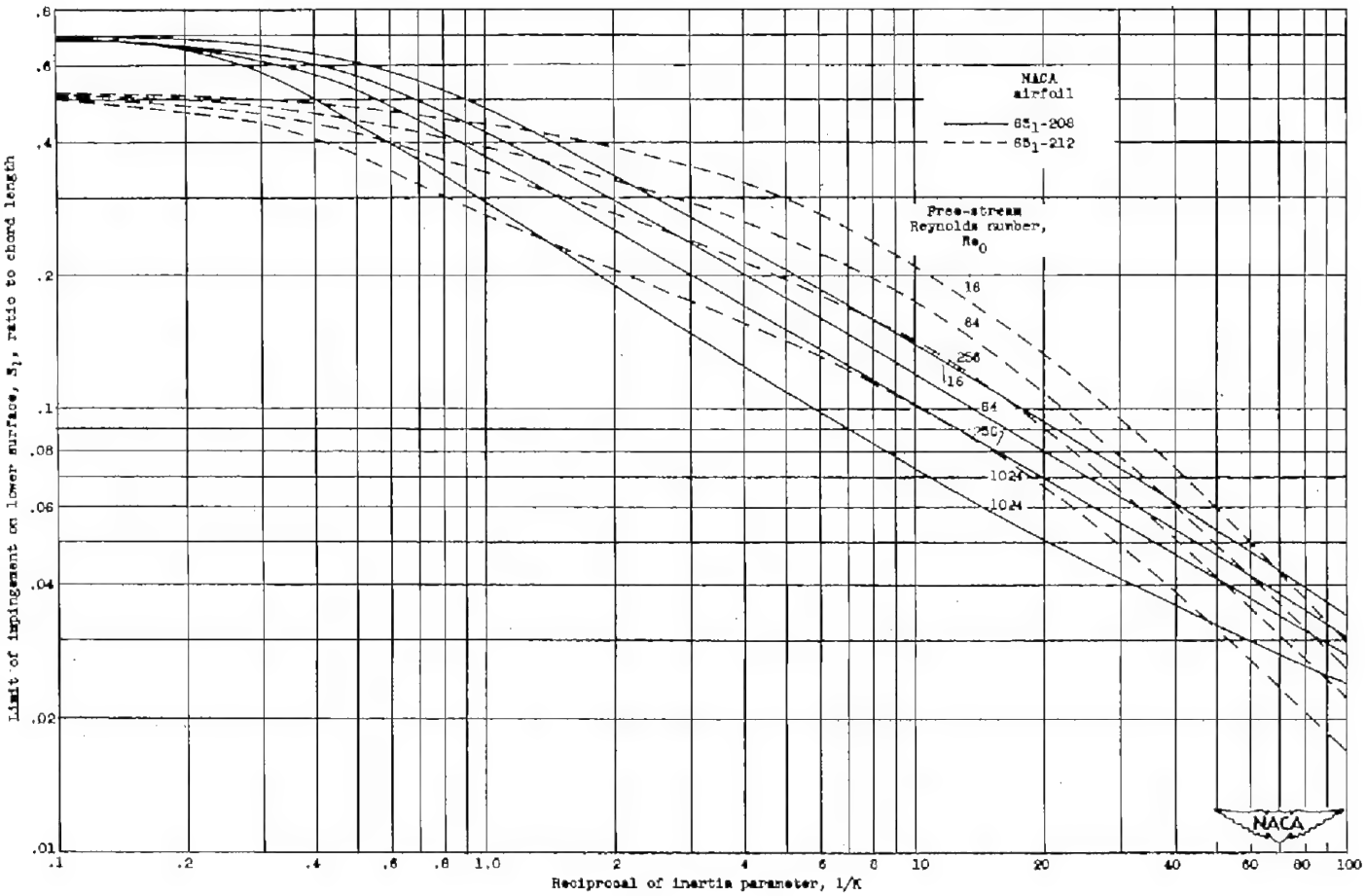

(b) Lower surface.

Figure 5. - Concluded. Limit of impingement on airfoil surface. Angle of attack, 4°.

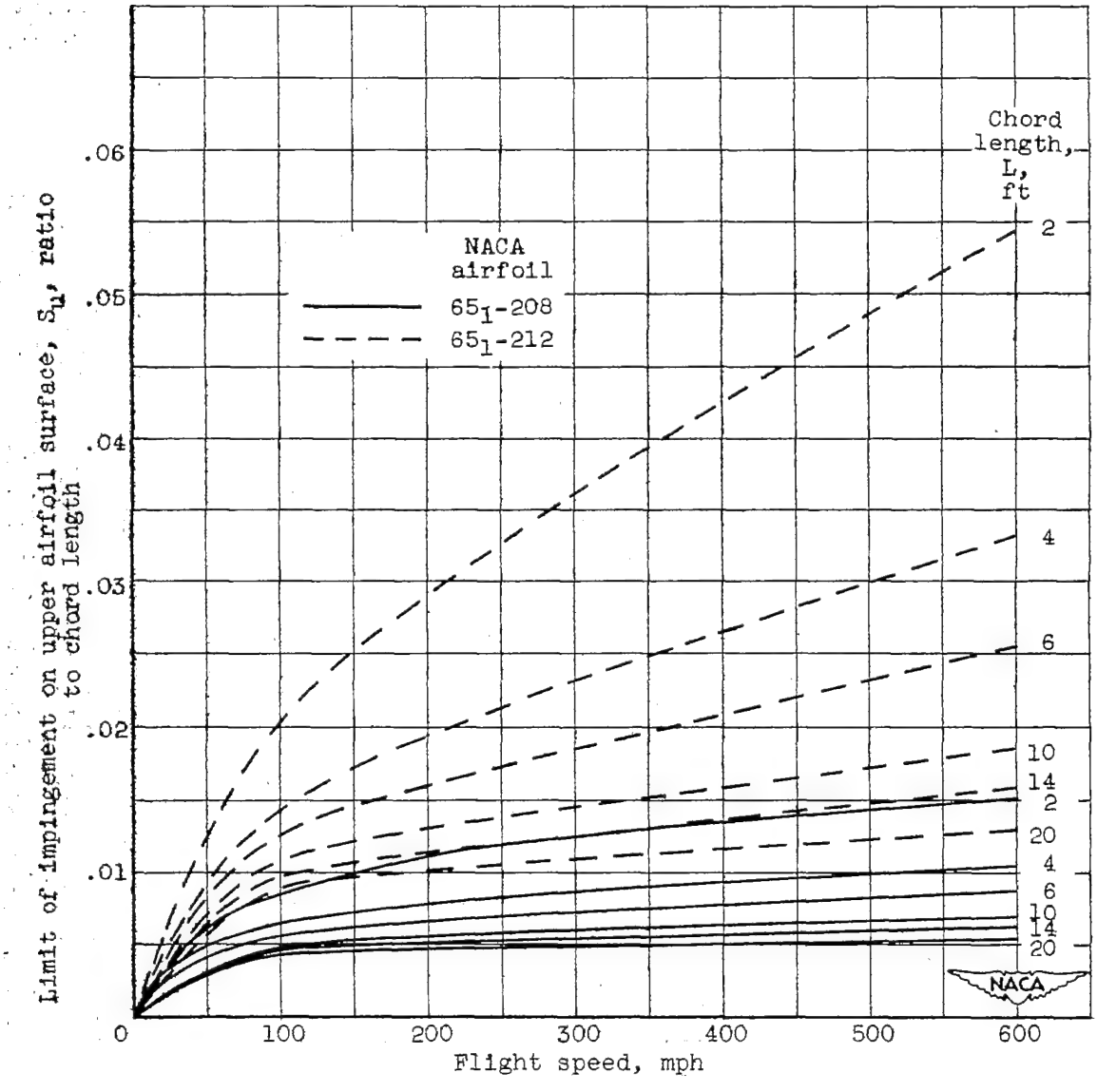

(a) Droplet size, 15 microns.

Figure 6. - Limit of impingement along upper surface. Altitude, 20,000 feet; angle of attack, 4°; most probable icing temperature, -11° F.

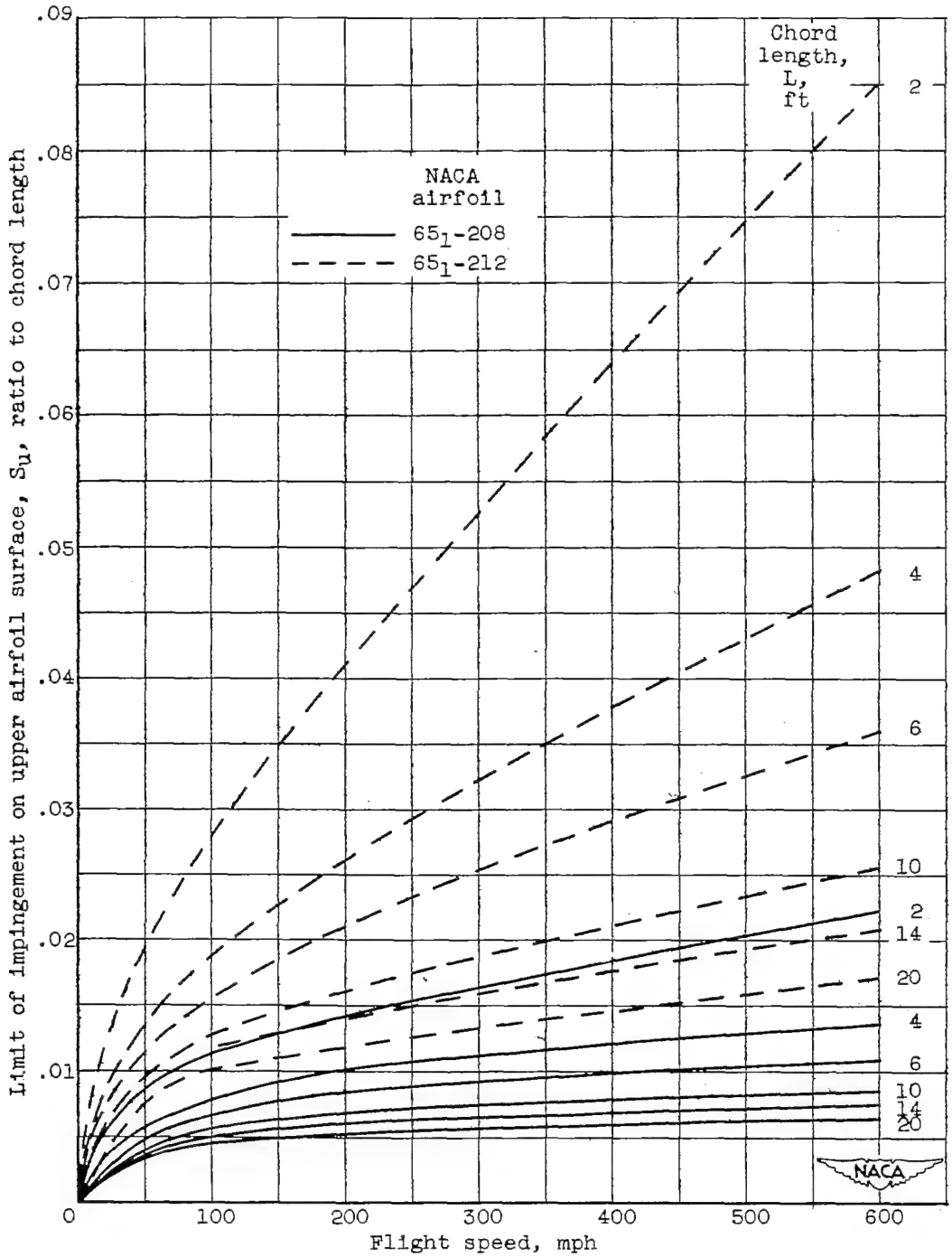

(b) Droplet size, 20 microns.

Figure 6. - Continued. Limit of impingement along upper surface. Altitude, 20,000 feet; angle of attack, 4°; most probable icing temperature, -11° F.

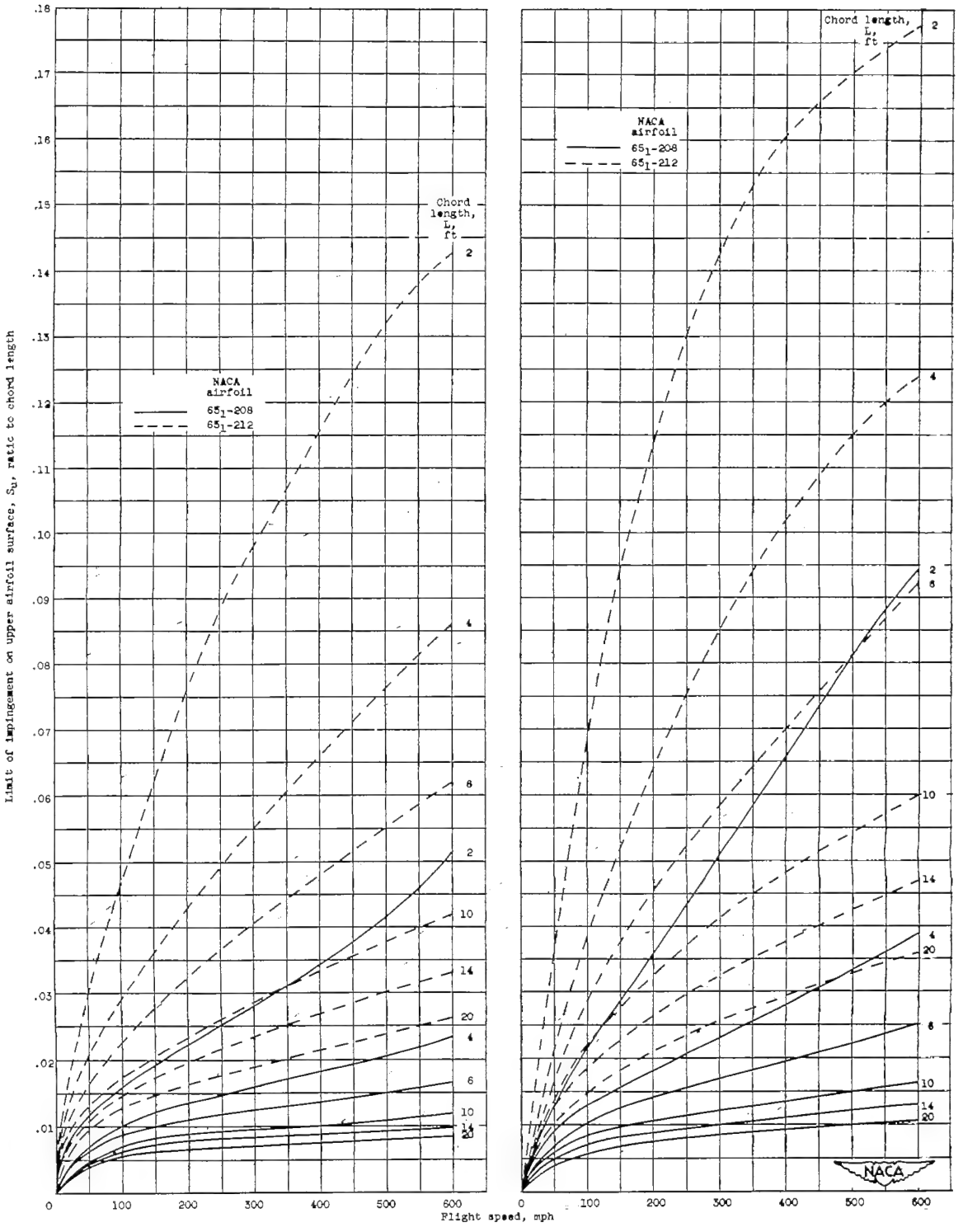

(c) Droplet size, 30 microns.

(d) Droplet size, 40 microns.

Figure 8. - Concluded. Limit of impingement along upper surface. Altitude, 20,000 feet; angle of attack, 4°; most probable icing temperature, -11° F.

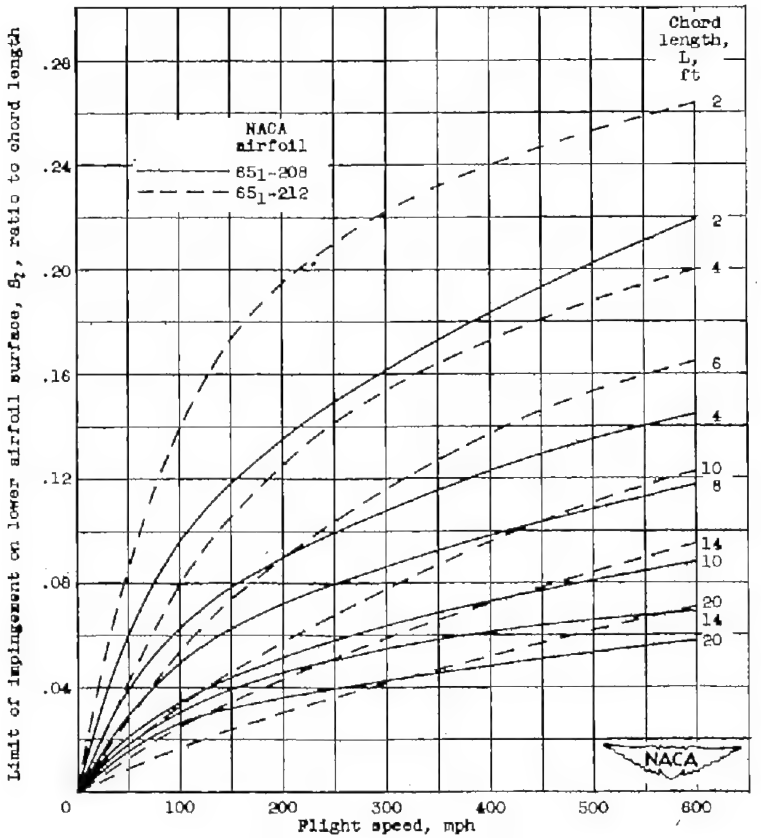

(a) Droplet size, 15 microns.

Figure 7. - Limit of impingement along lower surface. Altitude, 20,000 feet; angle of attack, 4°; most probable icing temperature, -11° F.

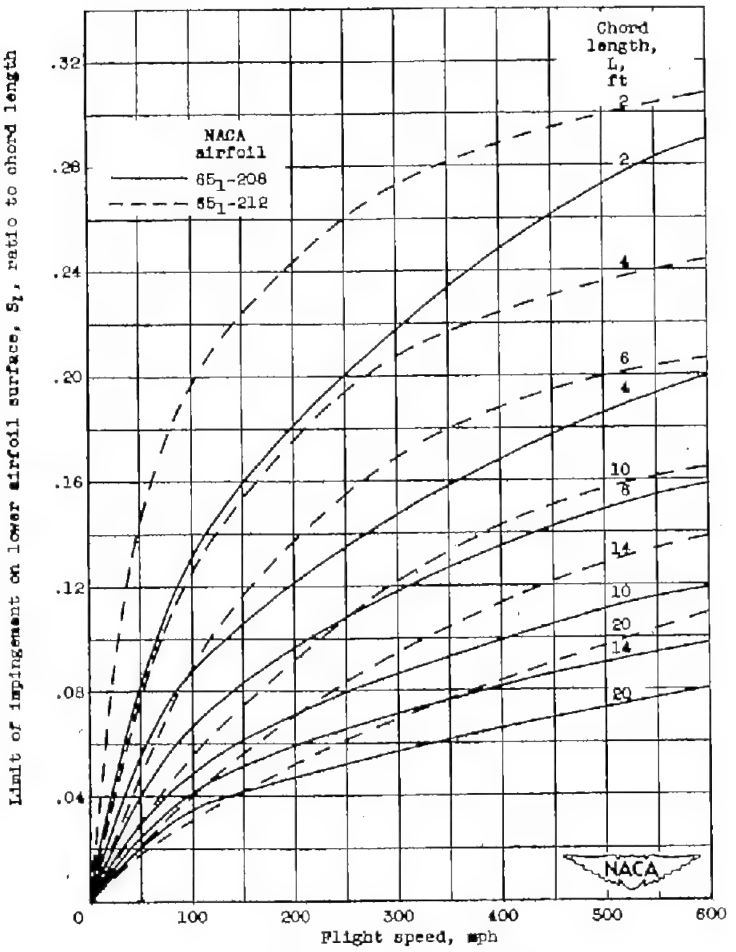

(b) Droplet size, 20 microns.

Figure 7. - Continued. Limit of impingement along lower surface. Altitude, 20,000 feet; angle of attack, 4°; most probable icing temperature, -11° F.

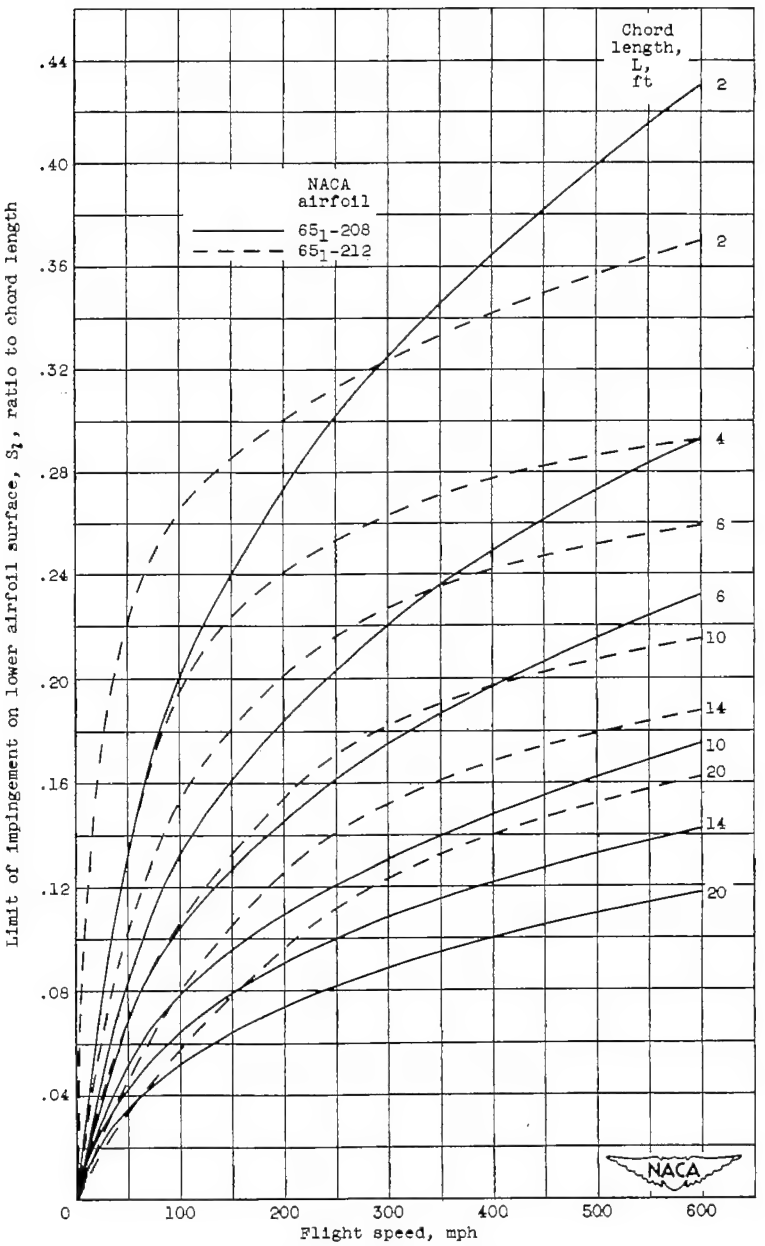

(c) Droplet size, 30 microns.

Figure 7. - Continued. Limit of impingement along lower surface. Altitude, 20,000 feet; angle of attack, 4°; most probable icing temperature, -11° F.

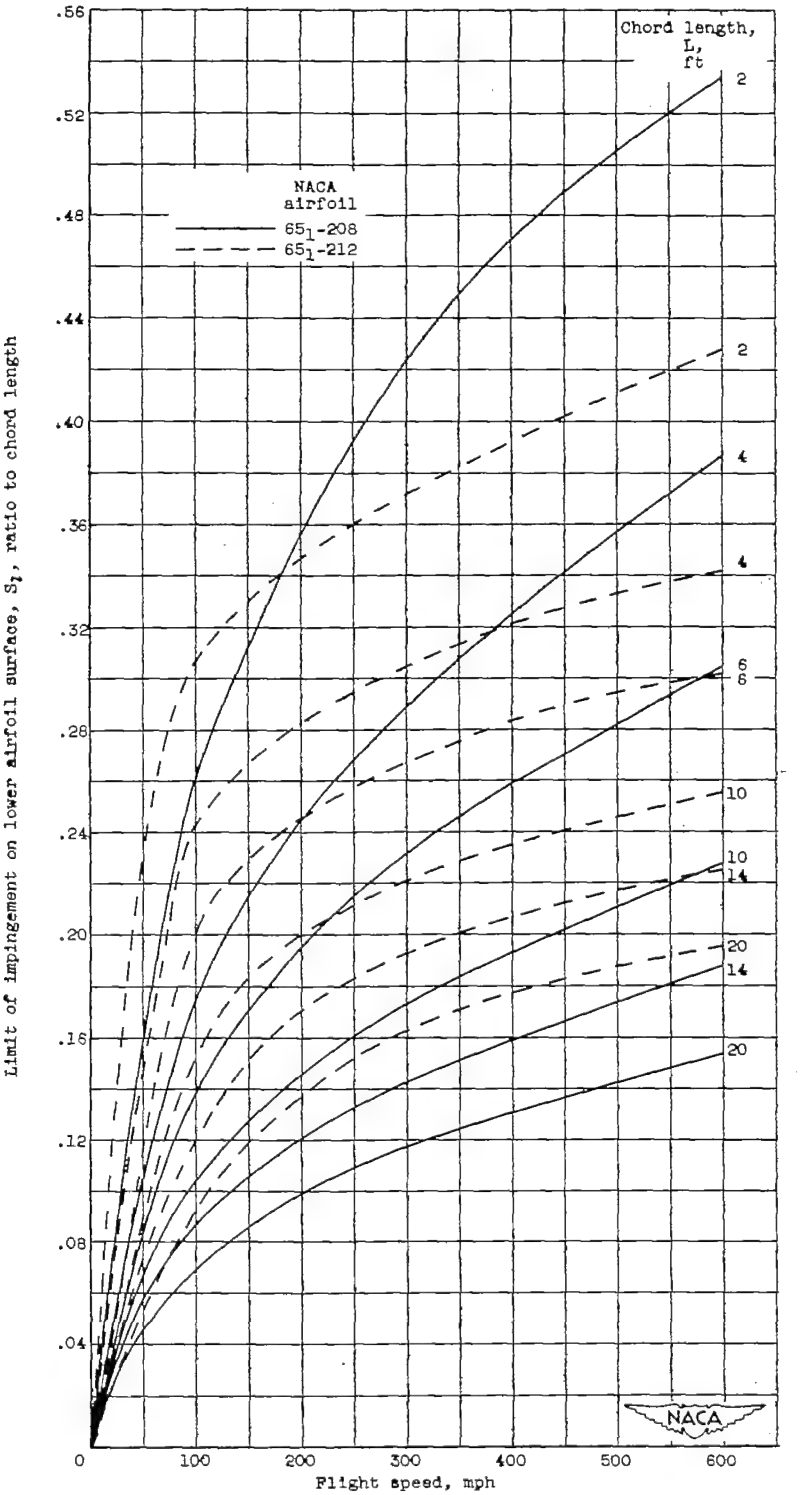

(d) Droplet size, 40 microns.

Figure 7. - Concluded. Limit of impingement along lower surface. Altitude, 20,000 feet; angle of attack, 4°; most probable icing temperature, -11° F.

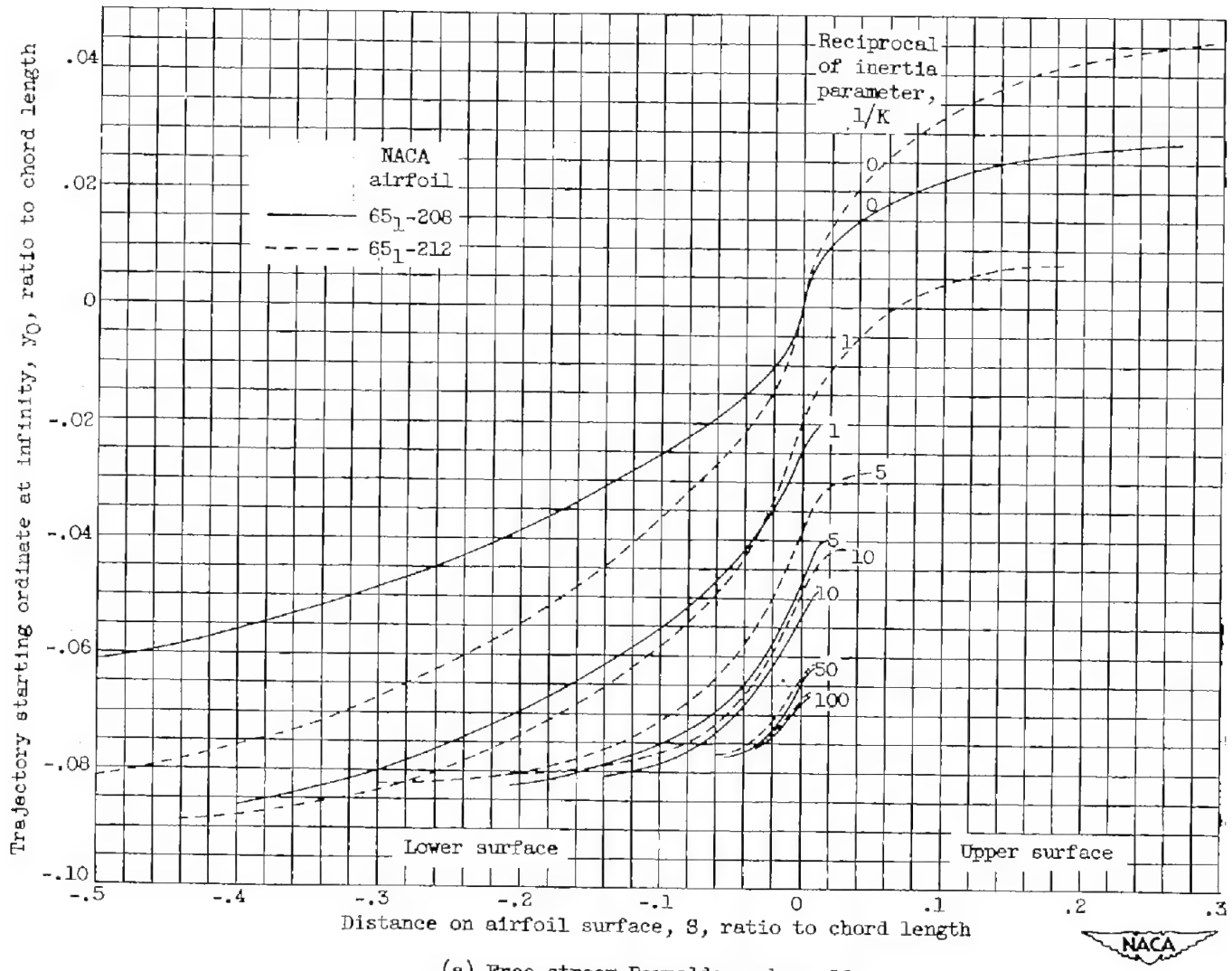

(a) Free-stream Reynolds number, 16.

Figure 8. - Trajectory starting ordinates as function of point of impingement on airfoil surface.

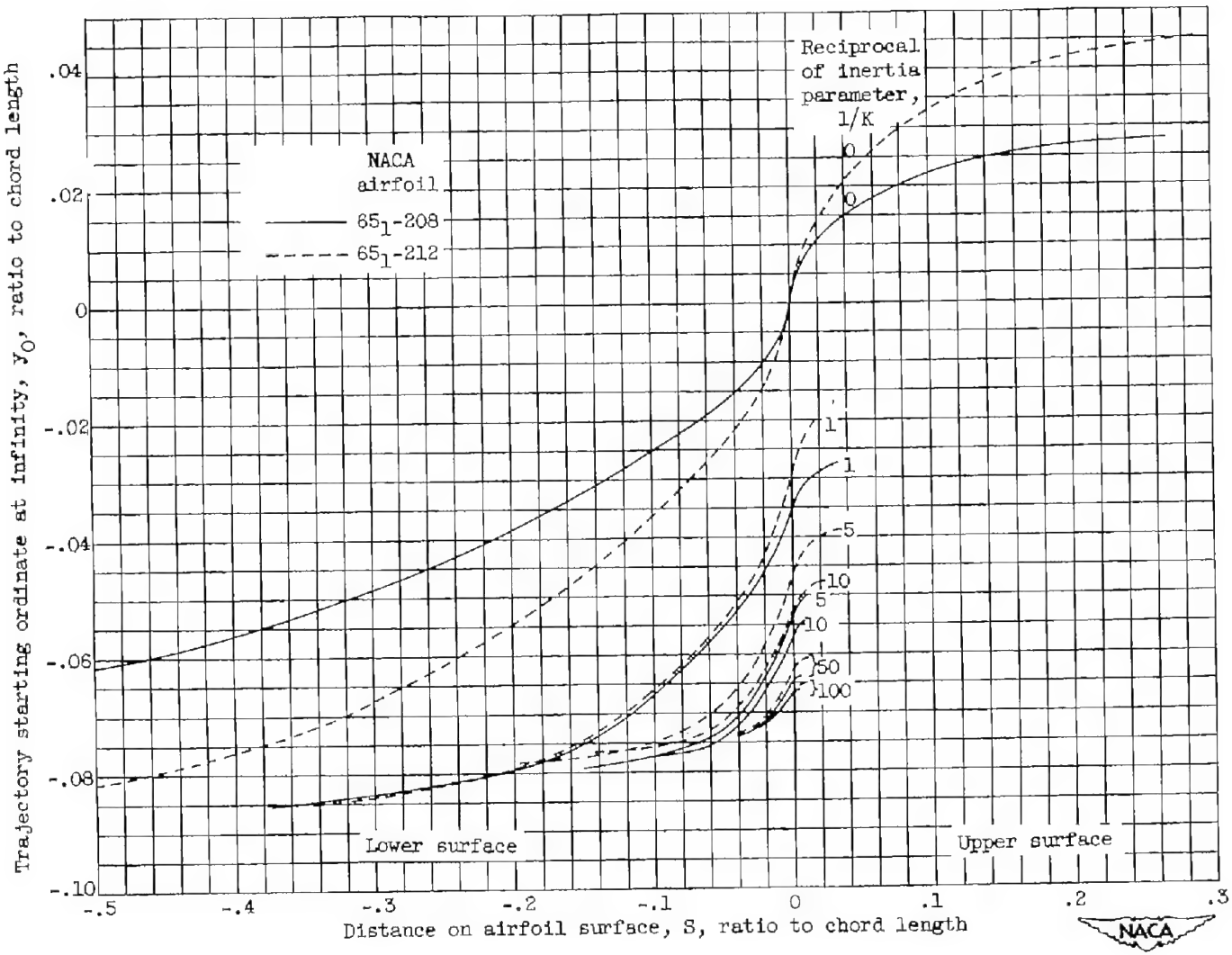

(b) Free-stream Reynolds number, 258.

Figure 8. - Continued. Trajectory starting ordinates as function of point of impingement on airfoil surface.

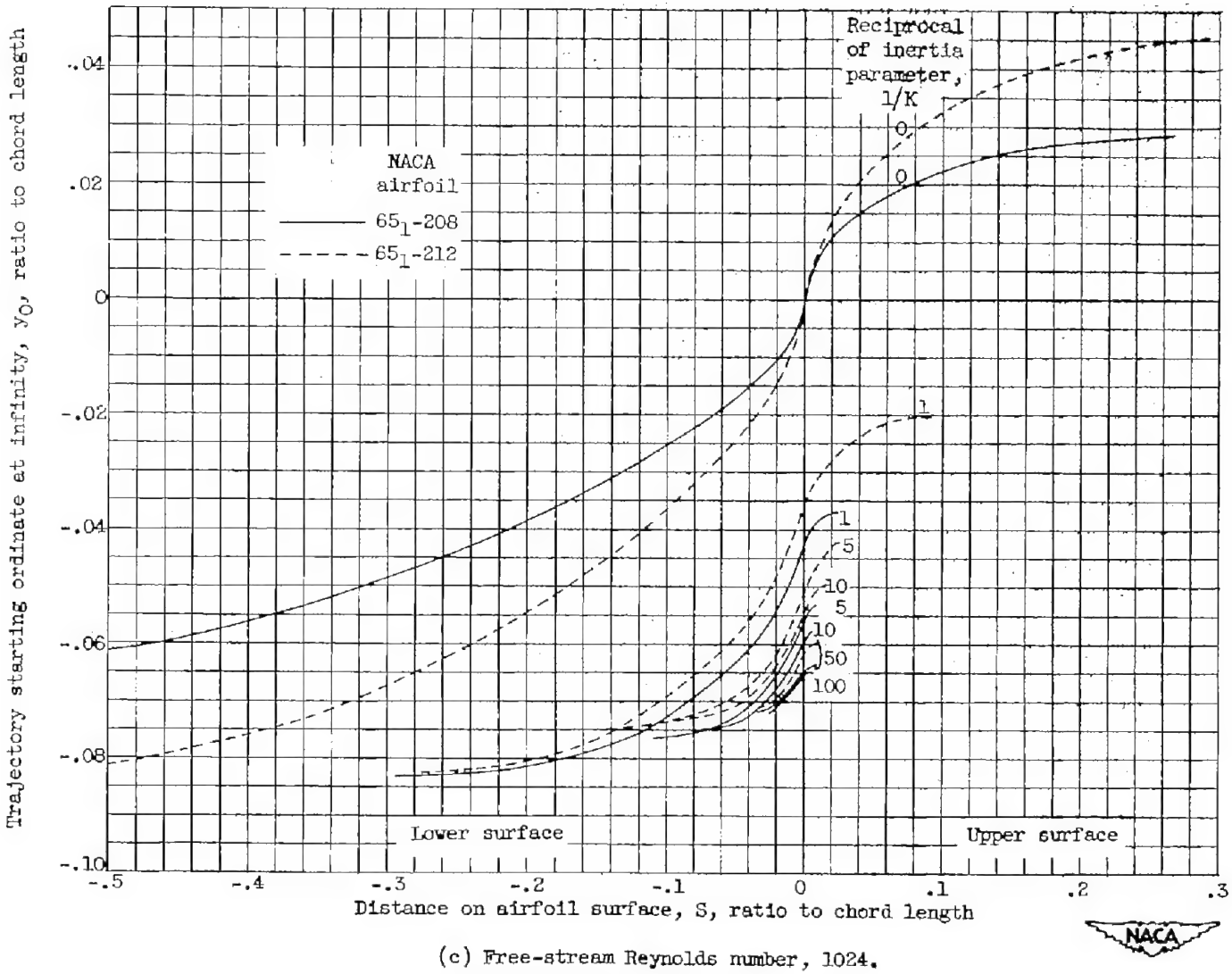

(c) Free-stream Reynolds number, 1024.

Figure 8. - Concluded. Trajectory starting ordinates as function of point of impingement on airfoil surface.

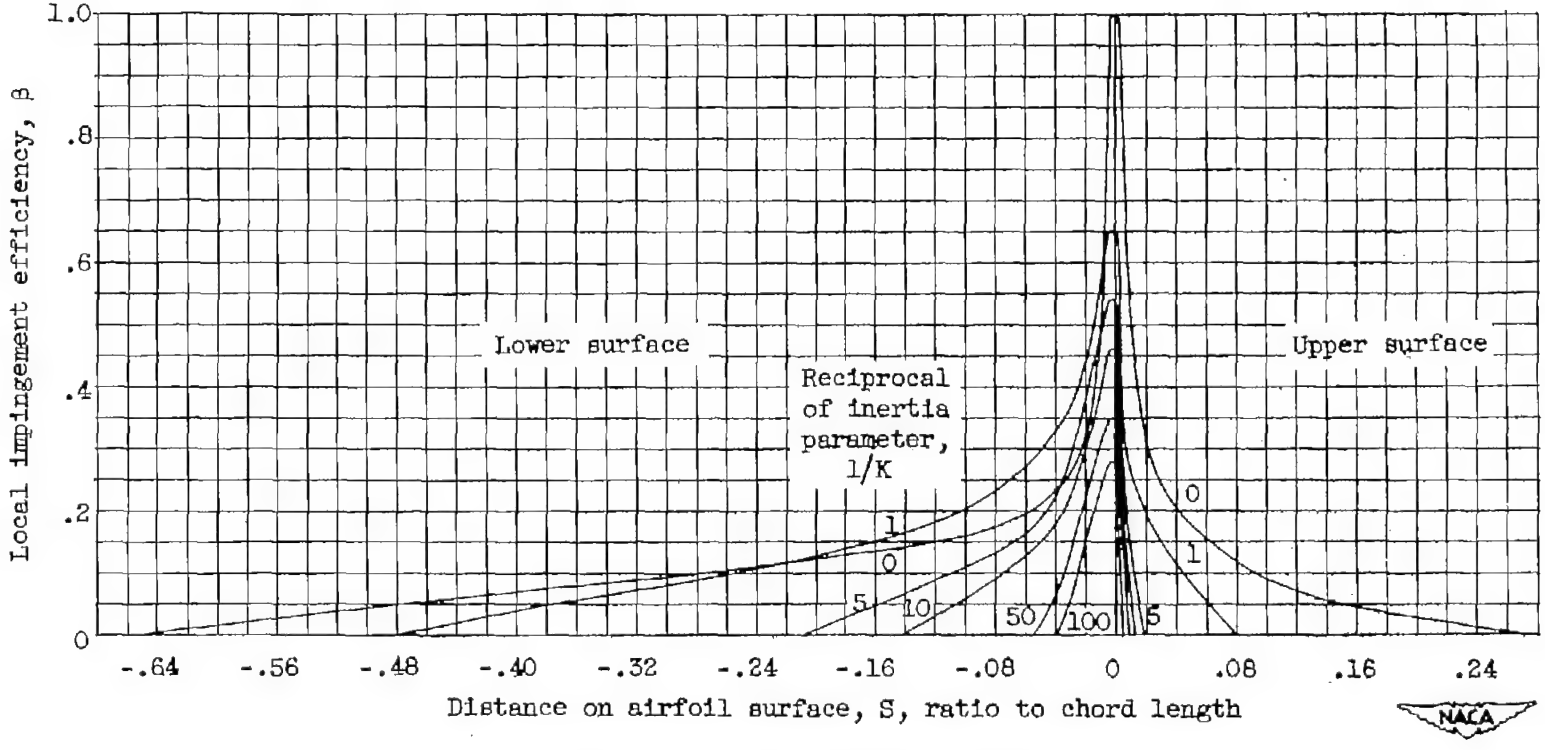

(a) Free-stream Reynolds number, 16.

Figure 9. - Local impingement efficiency. NACA 65_1-208 airfoil; angle of attack, 4°.

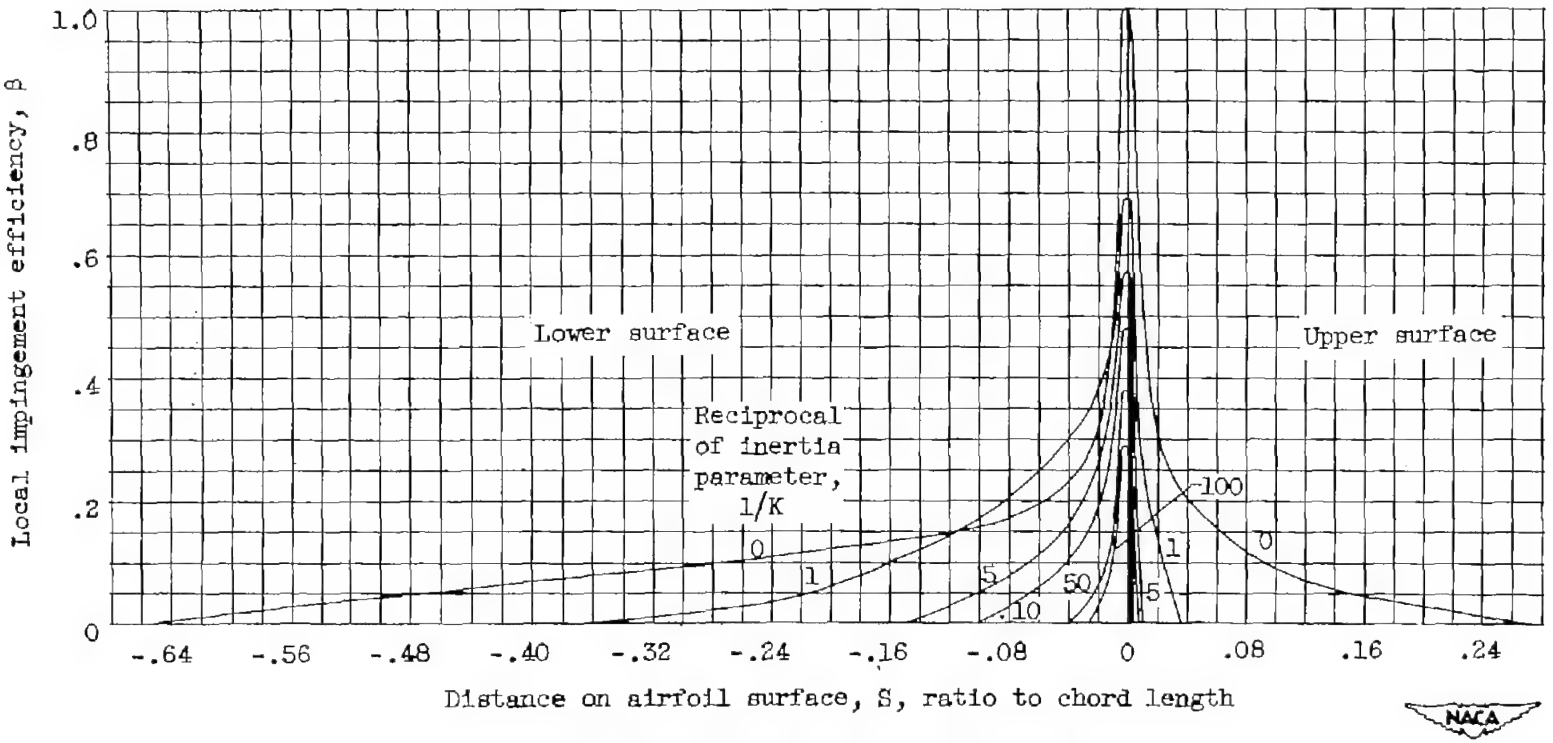

(b) Free-stream Reynolds number, 256.

Figure 9. - Continued. Local impingement efficiency. NACA 65_1-208 airfoil; angle of attack, 4°.

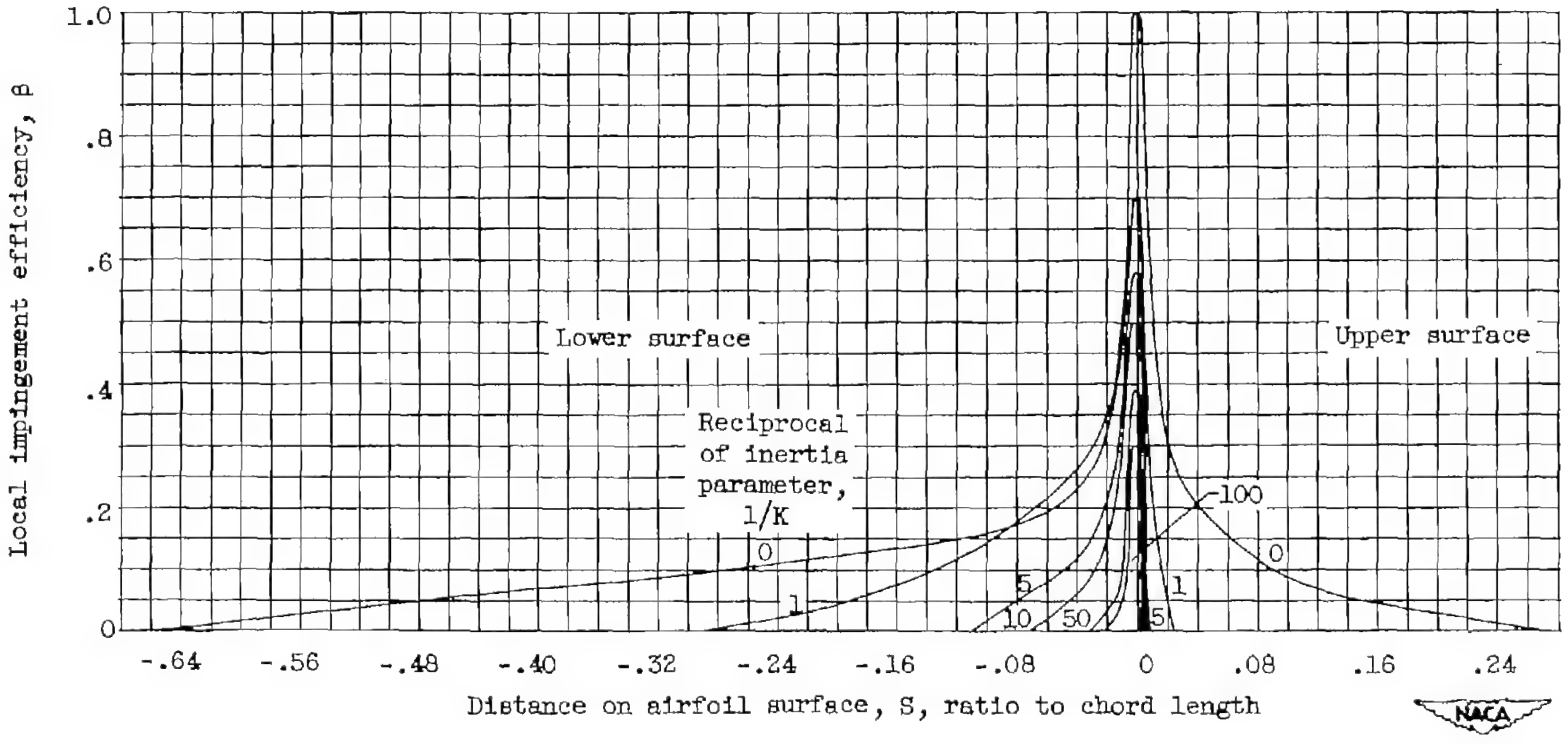

(c) Free-stream Reynolds number, 1024.

Figure 9. - Concluded. Local impingement efficiency. NACA 65_1-208 airfoil; angle of attack, 4°.

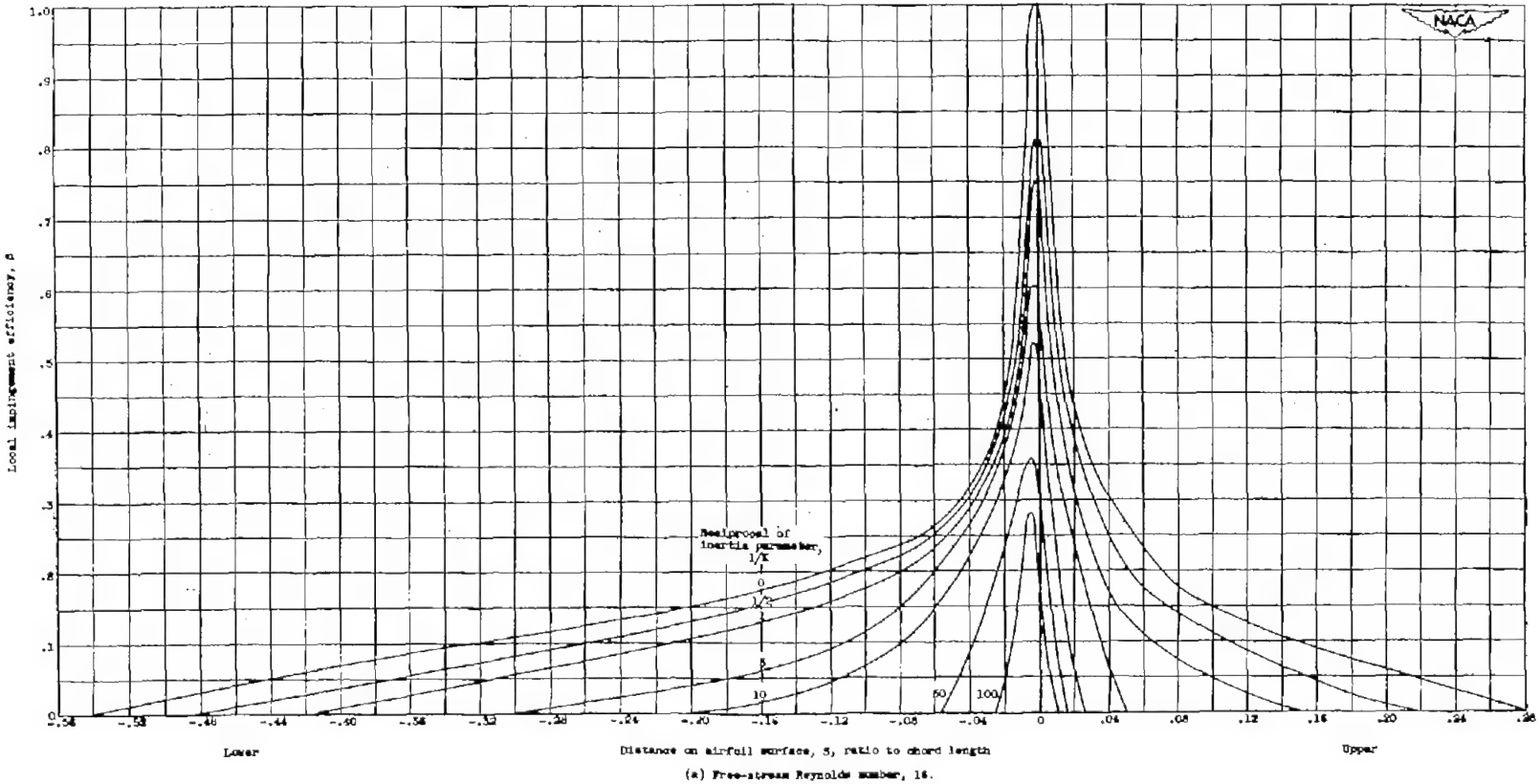

(a) Free-stream Reynolds number, 16.

Figure 10. - Local impingement efficiency. NACA 65_1-212 airfoil; angle of attack, 4°. (Reproduced from fig. 10, ref. 10.)

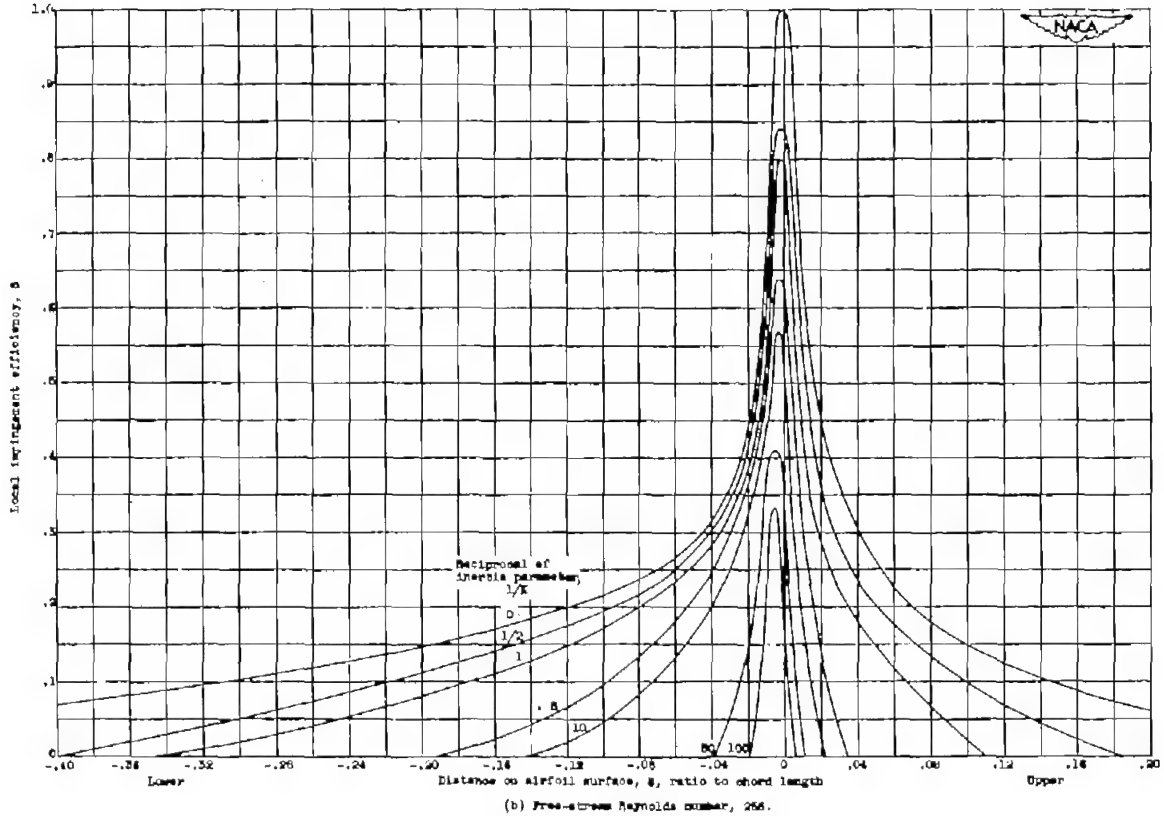

(b) Free-stream Reynolds number, 256.

Figure 10. - Continued. Local impingement efficiency. NACA 65_1-212 airfoil; angle of attack, 4°. (Reproduced from fig. 10, ref. 10.)

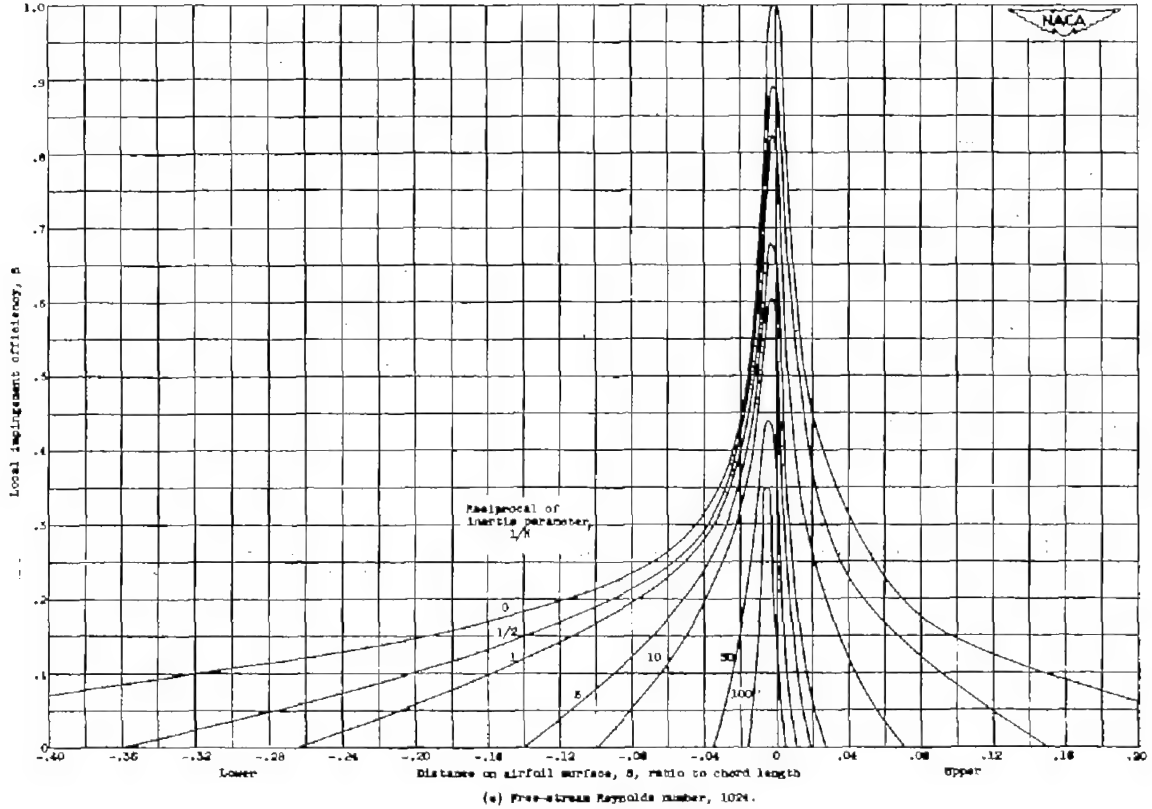

(a) Free-stream Reynolds number, 1024.

Figure 10. - Concluded. Local impingement efficiency. NACA 65_1-212 airfoil; angle of attack, 4°. (Reproduced from fig. 10, ref. 10.)

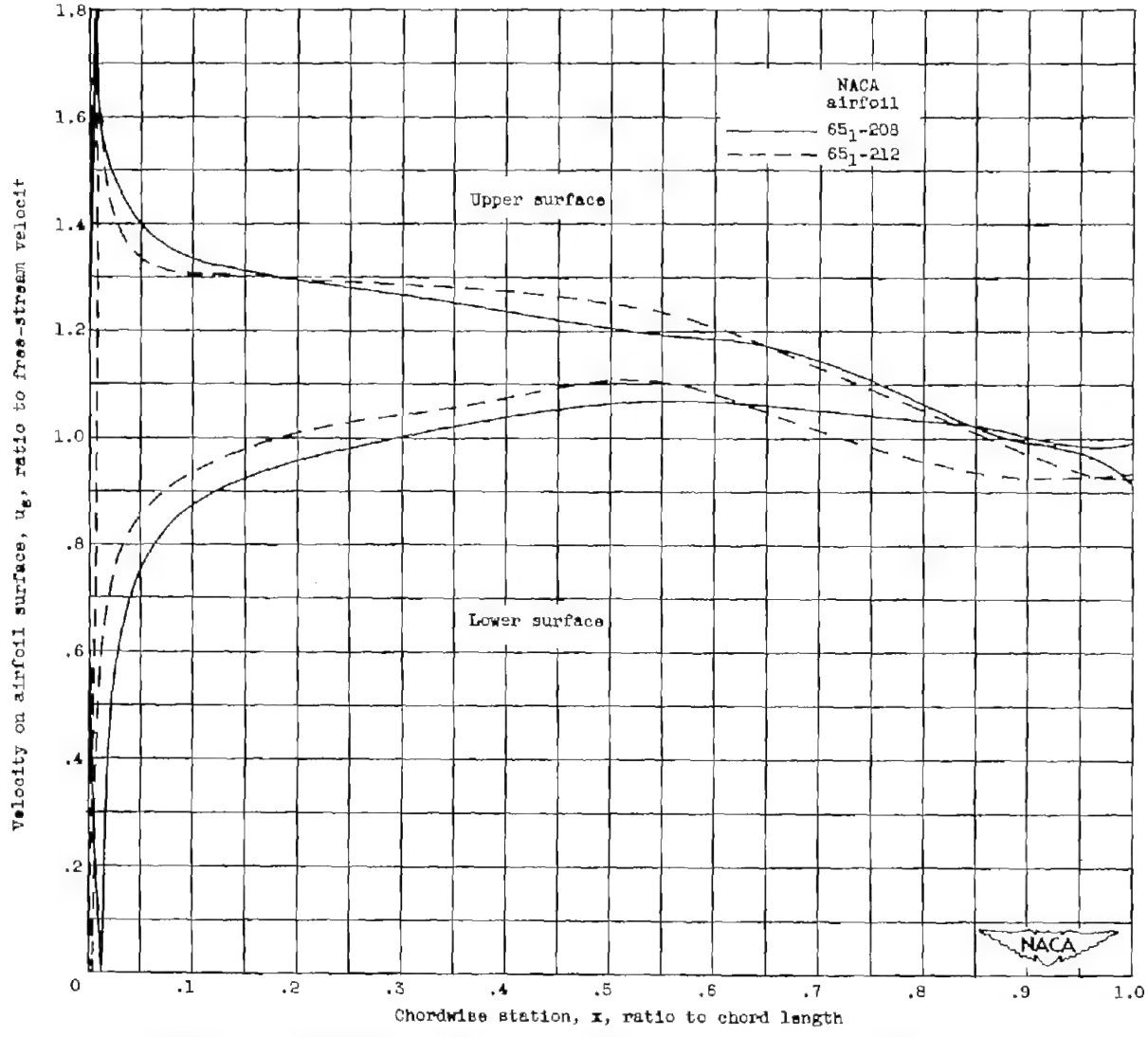

Figure 11. - Velocities on surface of two NACA 65-series airfoils. Angle of attack, 4°; free-stream Mach number, 0.2.

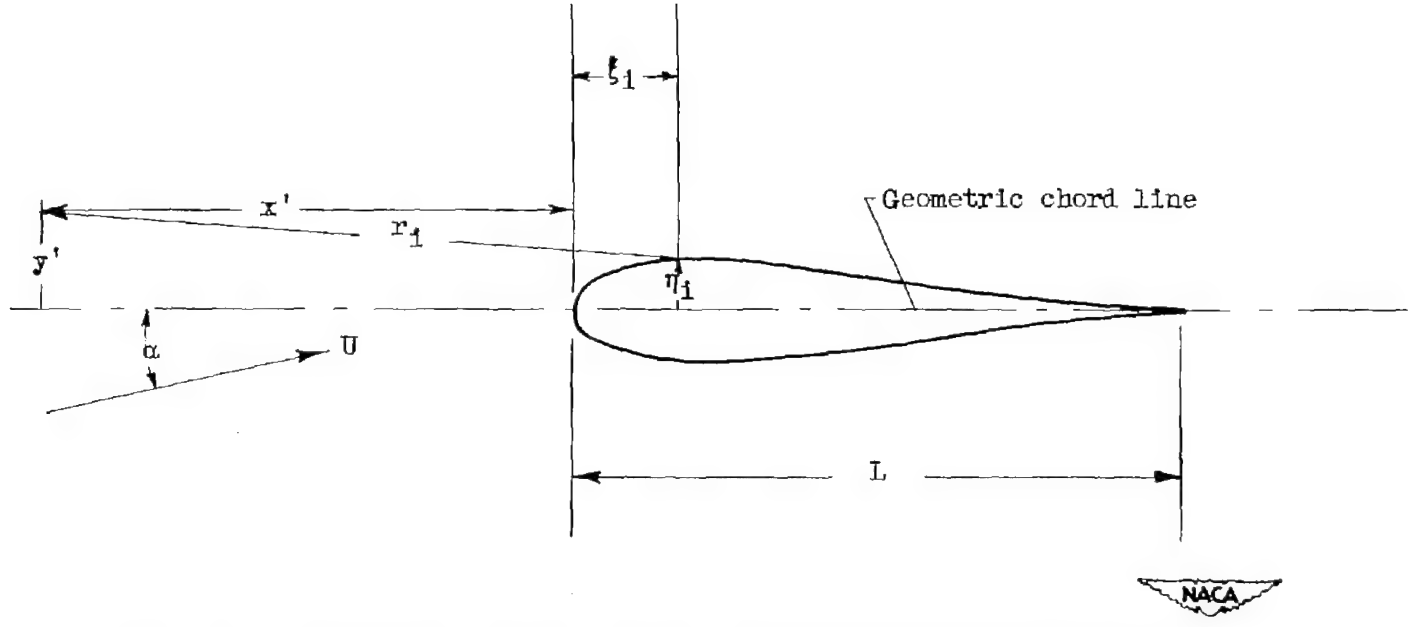

Figure 12. - Coordinate system used in computing flow-field velocities.

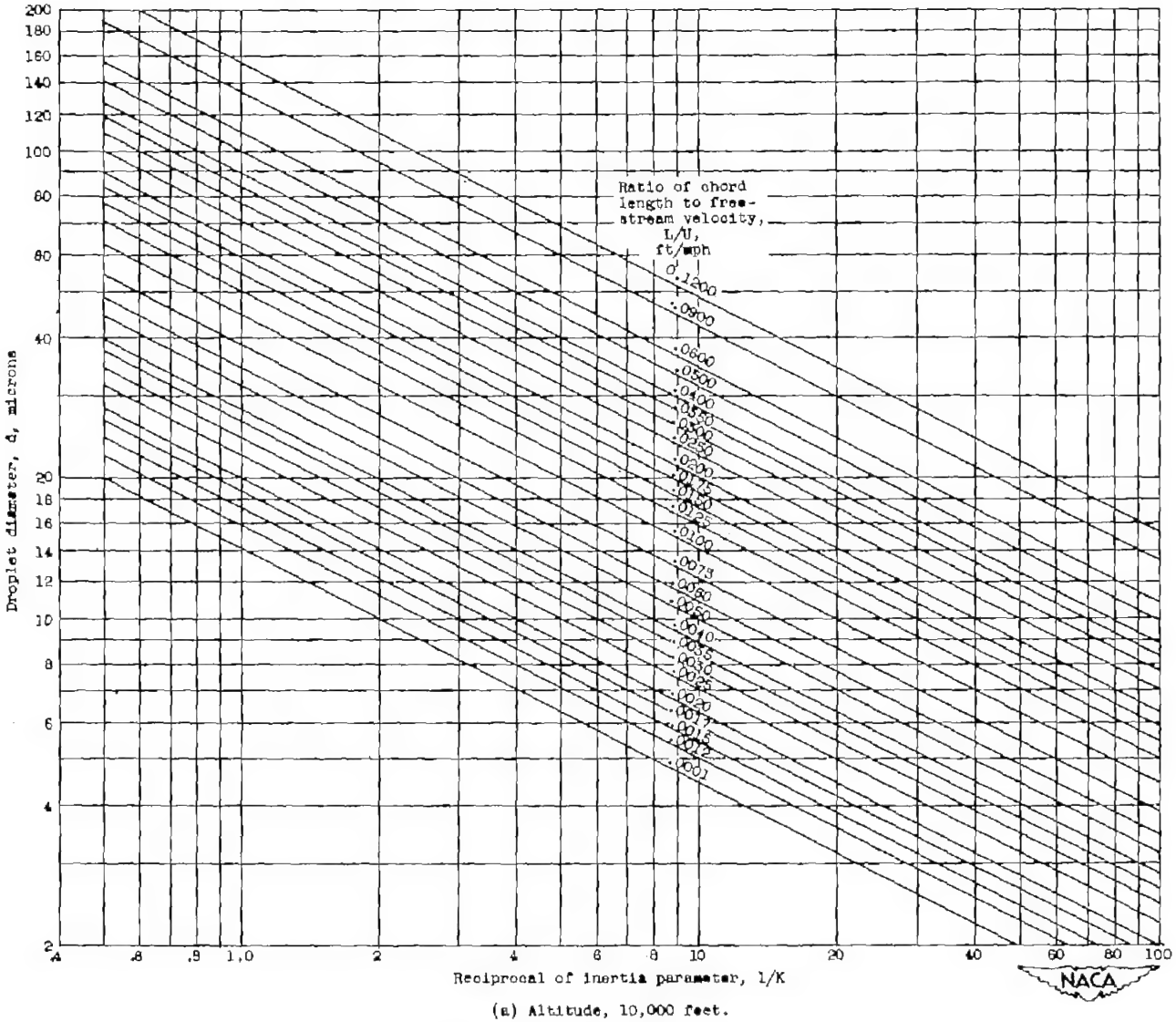

(a) Altitude, 10,000 feet.

Figure 13. - Droplet diameter as function of reciprocal of inertia parameter.

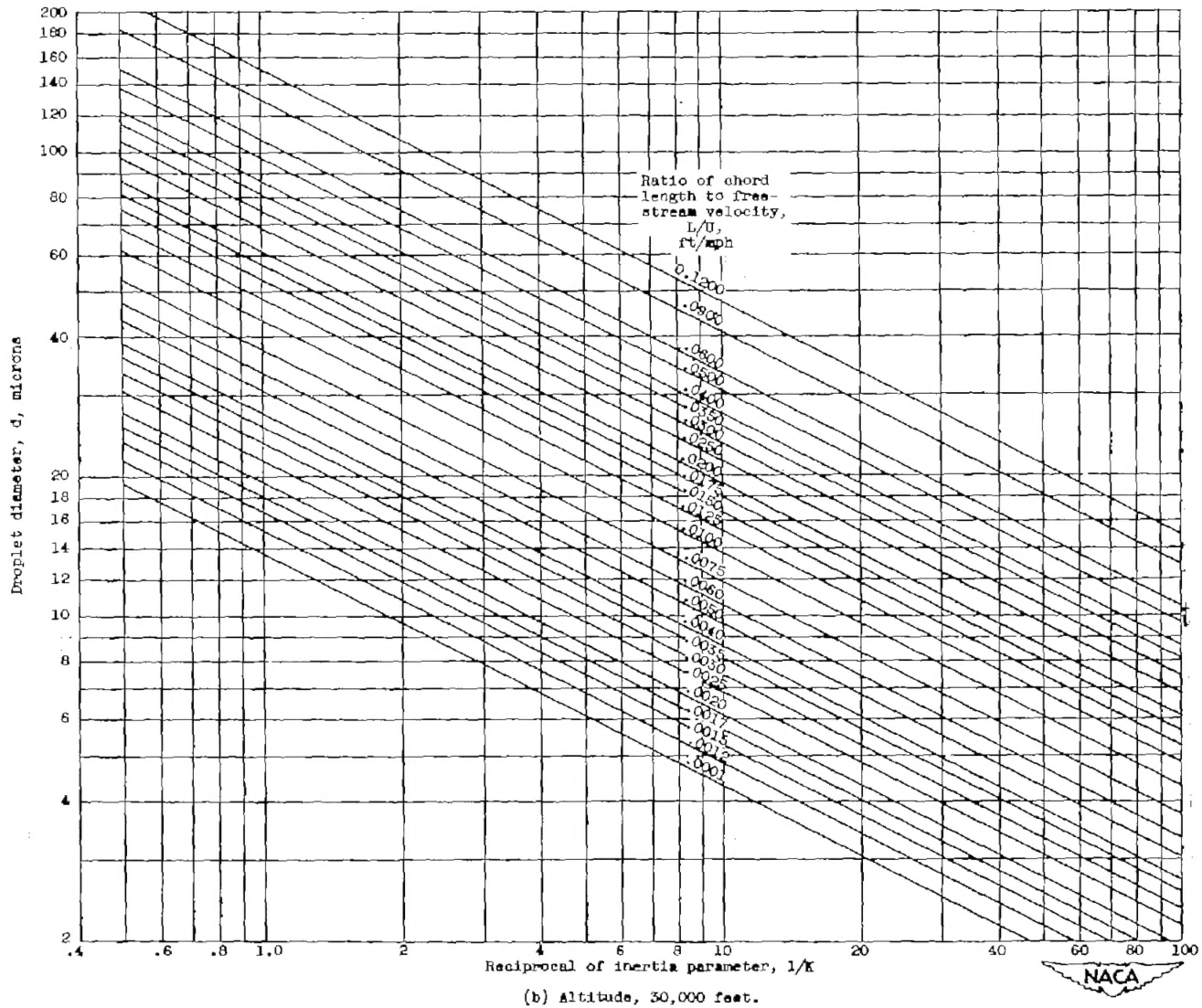

(b) Altitude, 30,000 feet.

Figure 13. - Concluded. Droplet diameter as function of reciprocal of inertia parameter.

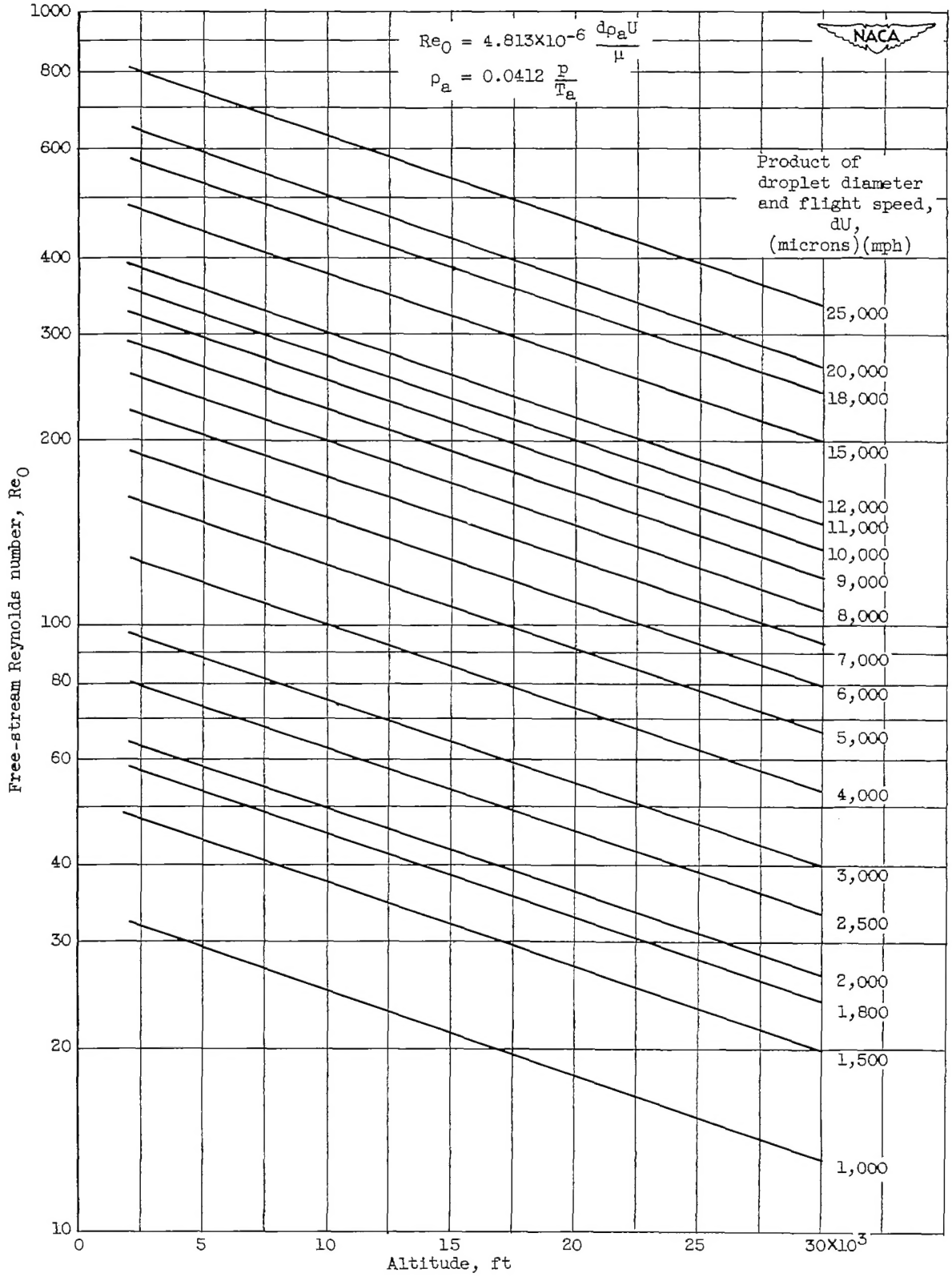

Figure 14. - Free-stream Reynolds number as function of altitude.

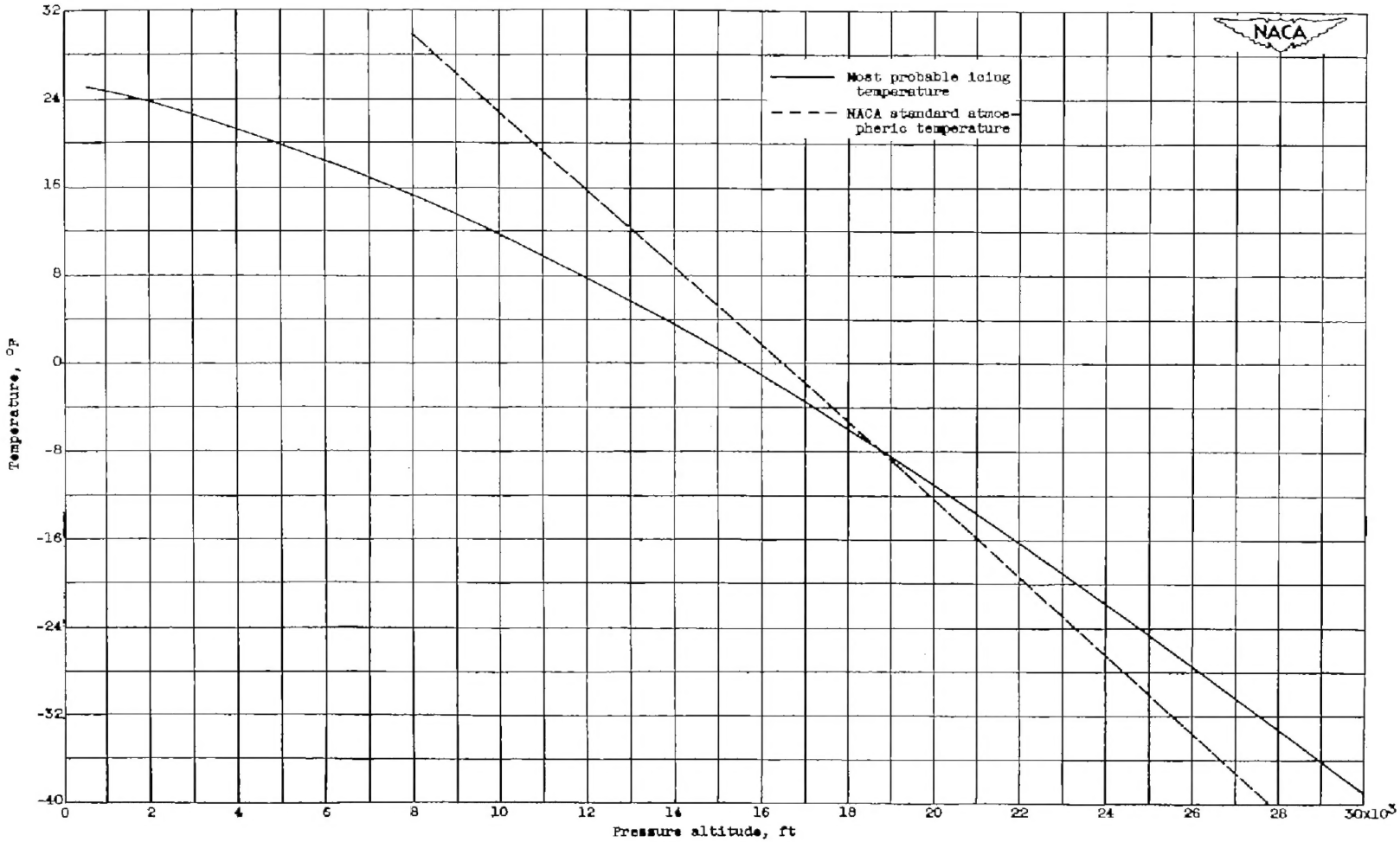

Figure 15. - Most probable icing temperature as function of pressure altitude. Most probable icing temperature at various altitudes obtained from approximately 300 icing observations (ref. 15). (Reproduced from fig. 14, ref. 10.)

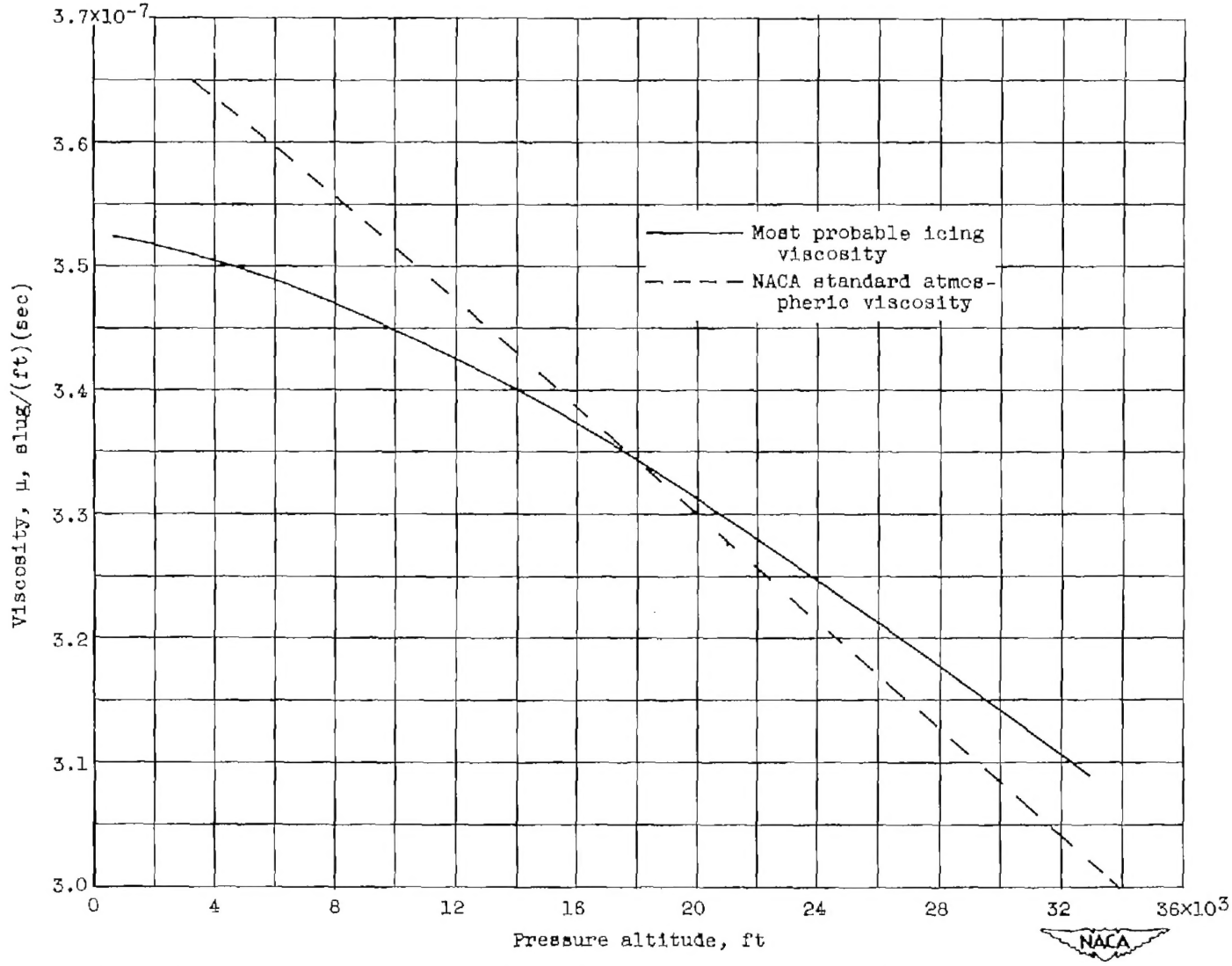

Figure 16. - Air viscosity as function of atmospheric altitude. (Based on most probable icing temperature.)